

**INTERPRETATIONS OF NEW AND PREVIOUS LEAD ISOTOPIC DATA FOR LATE  
CRETACEOUS TO EOCENE SATELLITE INTRUSIONS, BUTTE GRANITE,  
VOLCANIC ROCKS, AND BASE METAL VEINS OF THE BOULDER BATHOLITH,  
SOUTHWESTERN MONTANA**

Stanley L. Korzeb

*Montana Bureau of Mines and Geology, Butte, Montana*



*Cover photo: Kirk Waren, MBMG, Rampart Mountain.*

**INTERPRETATIONS OF NEW AND PREVIOUS LEAD ISOTOPIC DATA FOR LATE  
CRETACEOUS TO EOCENE SATELLITE INTRUSIONS, BUTTE GRANITE,  
VOLCANIC ROCKS, AND BASE METAL VEINS OF THE BOULDER BATHOLITH,  
SOUTHWESTERN MONTANA**

Stanley L. Korzeb

*Montana Bureau of Mines and Geology, Butte, Montana*





## CONTENTS

Abstract .....	1
Introduction .....	2
Geologic Setting .....	3
Previous Investigations .....	5
Analytical Procedures .....	6
Results .....	7
Discussion .....	9
Base Metal Veins .....	13
Satellite Plutons and Intrusions .....	14
Lowland Creek Volcanic Field .....	14
Elkhorn Mountains Volcanic Field .....	17
Stream Sediments .....	17
Big Belt Mountains .....	18
Belt Supergroup Formations and Sulfide Veins .....	19
Magma Source .....	23
Ore Deposit Genesis .....	27
Conclusion .....	29
Acknowledgments .....	29
References .....	30
Appendix A .....	33
Appendix B .....	35
Appendix C .....	36
Appendix D .....	37
Appendix E .....	38
Appendix F .....	40

## FIGURES

Figure 1. Geologic map of Boulder Batholith showing mining districts and approximate locations for base metal vein galena samples .....	4
Figure 2. Covariant diagram of $^{206}\text{Pb}/^{204}\text{Pb}$ vs. $^{207}\text{Pb}/^{204}\text{Pb}$ plot for base metal vein and breccia pipe galena lead isotope ratios generated by this investigation .....	7
Figure 3. Covariant diagram of $^{206}\text{Pb}/^{204}\text{Pb}$ vs. $^{207}\text{Pb}/^{204}\text{Pb}$ plot for Boulder Batholith intrusions published by Doe and others (1968) with added data generated by this investigation .....	8
Figure 4. Covariant diagram of $^{206}\text{Pb}/^{204}\text{Pb}$ vs. $^{207}\text{Pb}/^{204}\text{Pb}$ plot for Lowland Creek volcanic rocks published by Dudás and others (2010) with added data generated by this investigation .....	8
Figure 5. Covariant diagram of $^{206}\text{Pb}/^{204}\text{Pb}$ vs. $^{207}\text{Pb}/^{204}\text{Pb}$ plot for Elkhorn Mountains volcanic rocks published by Doe and others (1968) with added data generated by this investigation .....	9
Figure 6. Covariant diagram of $^{206}\text{Pb}/^{204}\text{Pb}$ vs. $^{207}\text{Pb}/^{204}\text{Pb}$ plot for Basin Mining district stream sediment samples published by Uhrh and others (2000) .....	10
Figure 7. Covariant diagram of $^{206}\text{Pb}/^{204}\text{Pb}$ vs. $^{207}\text{Pb}/^{204}\text{Pb}$ plot for the Big Belt Mountains published by du Bray and others (2017) .....	11

Figure 8. Covariant diagram of $^{206}\text{Pb}/^{204}\text{Pb}$ vs. $^{207}\text{Pb}/^{204}\text{Pb}$ plot for the Belt Supergroup formations and sulfide veins published by Zartman (1992).....	11
Figure 9. Covariant diagram for $^{208}\text{Pb}/^{204}\text{Pb}$ vs. $^{206}\text{Pb}/^{204}\text{Pb}$ plot for base metal vein and breccia pipe galena lead isotope data generated by this investigation.....	13
Figure 10. Covariant diagram for $^{208}\text{Pb}/^{204}\text{Pb}$ vs. $^{206}\text{Pb}/^{204}\text{Pb}$ plot for Boulder Batholith intrusions published by Doe and others (1968) with additional data generated by this investigation.....	15
Figure 11. Covariant diagram for $^{208}\text{Pb}/^{204}\text{Pb}$ vs. $^{206}\text{Pb}/^{204}\text{Pb}$ plot for Lowland Creek volcanic rocks published by Dudás and others (2010) with additional data generated by this investigation.....	16
Figure 12. Covariant diagram for $^{208}\text{Pb}/^{204}\text{Pb}$ vs. $^{206}\text{Pb}/^{204}\text{Pb}$ plot for Elkhorn Mountains volcanic rocks published by Doe and others (1968) with additional data generated by this investigation ...	17
Figure 13. Covariant diagram for $^{208}\text{Pb}/^{204}\text{Pb}$ vs. $^{206}\text{Pb}/^{204}\text{Pb}$ plot for stream sediment samples from the Basin mining district (Uhruh and others, 2000) .....	18
Figure 14. Covariant diagram for $^{208}\text{Pb}/^{204}\text{Pb}$ vs. $^{206}\text{Pb}/^{204}\text{Pb}$ plot for the Big Belt Mountains, data published by du Bray and others (2017) .....	19
Figure 15. Covariant diagram for $^{208}\text{Pb}/^{204}\text{Pb}$ vs. $^{206}\text{Pb}/^{204}\text{Pb}$ plot for the Belt Supergroup formations and hosted sulfide veins, data published by Zartman (1992).....	20
Figure 16. Lead isotope ratios generated by this investigation for galena samples from base metal veins and galena from Montana Tunnels breccia pipe plotted on Stacey and Kramers (1975) model lead isotope growth curves for $^{206}\text{Pb}/^{204}\text{Pb}$ vs. $^{207}\text{Pb}/^{204}\text{Pb}$ (below) and $^{206}\text{Pb}/^{204}\text{Pb}$ vs. $^{208}\text{Pb}/^{204}\text{Pb}$ ratios.....	21
Figure 17. Lead isotope ratios for Boulder Batholith intrusions from data published by Doe and others (1968) with additional data generated by this investigation (red points) plotted on Stacey and Kramers (1975) model lead isotope growth curves for $^{206}\text{Pb}/^{204}\text{Pb}$ vs. $^{207}\text{Pb}/^{204}\text{Pb}$ (below) and $^{206}\text{Pb}/^{204}\text{Pb}$ vs. $^{208}\text{Pb}/^{204}\text{Pb}$ ratios.....	22
Figure 18. Lead isotope ratios for Lowland Creek volcanic rocks from data published by Dudás and others (2010) with additional data generated by this investigation (red points) plotted on Stacey and Kramers (1975) model lead isotope growth curves for $^{206}\text{Pb}/^{204}\text{Pb}$ vs. $^{207}\text{Pb}/^{204}\text{Pb}$ (below) and $^{206}\text{Pb}/^{204}\text{Pb}$ vs. $^{208}\text{Pb}/^{204}\text{Pb}$ ratios.....	23
Figure 19. Lead isotope ratios for Elkhorn Mountains volcanic rocks from data published by Doe and others (1968) with additional data generated by this investigation (red points) plotted on Stacey and Kramers (1975) model lead isotope growth curves for $^{206}\text{Pb}/^{204}\text{Pb}$ vs. $^{207}\text{Pb}/^{204}\text{Pb}$ (below) and $^{206}\text{Pb}/^{204}\text{Pb}$ vs. $^{208}\text{Pb}/^{204}\text{Pb}$ ratios.....	24
Figure 20. Lead isotope ratios for stream sediments from the Basin mining district from data published by Uhruh and others (2000) plotted on Stacey and Kramers (1975) model lead isotope growth curves for $^{206}\text{Pb}/^{204}\text{Pb}$ vs. $^{207}\text{Pb}/^{204}\text{Pb}$ (below) and $^{208}\text{Pb}/^{204}\text{Pb}$ vs. $^{206}\text{Pb}/^{204}\text{Pb}$ ratios .....	25
Figure 21. Lead isotope ratios for the Big Belt Mountains from data published by du Bray and others (2017) plotted on Stacey and Kramers (1975) model lead isotope growth curves for $^{206}\text{Pb}/^{204}\text{Pb}$ vs. $^{207}\text{Pb}/^{204}\text{Pb}$ (below) and $^{206}\text{Pb}/^{204}\text{Pb}$ vs. $^{208}\text{Pb}/^{204}\text{Pb}$ ratios .....	26
Figure 22. Lead isotope ratios for Belt Supergroup formations and hosted sulfide veins from data published by Zartman (1992) plotted on Stacey and Kramers (1975) model lead isotope growth curves for $^{206}\text{Pb}/^{204}\text{Pb}$ vs. $^{207}\text{Pb}/^{204}\text{Pb}$ (below) and $^{206}\text{Pb}/^{204}\text{Pb}$ vs. $^{208}\text{Pb}/^{204}\text{Pb}$ ratios.....	28

## TABLE

Table 1. Summary of lead isotope ranges for samples showing degrees of compatible isotope signatures.....	14
---	----

## ABSTRACT

New lead isotope data generated from this investigation were used in conjunction with data from previous investigations to identify a metal source for the Boulder Batholith base metal veins and a magmatic source for the Butte Granite, Boulder Batholith satellite plutons, and associated volcanic fields. To constrain the lead isotope data, covariant plots generated from 2.7 Ga initial lead isotope data for Stillwater and lead isotope data from the Big Belt Mountains were used. Lead isotope data for the base metal veins, satellite plutons, Butte Granite, Elkhorn Mountains, and Lowland Creek volcanic rocks overlap, indicating a common source. This data set plotted on covariant diagrams follows an 85 Ma mixing line with lead isotopes sourced from both a subcontinent lithospheric component and upper crust. Lead isotopes suggest the magmas that generated the Boulder Batholith intrusions and associated volcanic rocks originated from Archean–Proterozoic mafic to intermediate basement that assimilated upper crust. The variations in  $^{207}\text{Pb}/^{204}\text{Pb}$  and  $^{208}\text{Pb}/^{204}\text{Pb}$  between different intrusions and volcanic rocks indicate a heterogeneous isotopic source. Past investigations suggest assimilated upper crust contributed inherited zircons to the intrusions with Proterozoic cores, and Cretaceous age rims and base metal veins have sulfur isotopes with Belt Supergroup signatures. Proximity and Cretaceous ages of the Boulder Batholith and Big Belt Mountains imply both originated from the same geologic process of subduction-related magmatism, including mantle-derived components.

Lead isotopes for base metal vein galena samples overlap the intrusions and volcanic rocks hosting the veins, are in isotopic equilibrium, and share a common isotopic source. Overlapping of Pb isotopes for the base metal veins, intrusions, and volcanic rocks imply the Pb isotopic source for the base metal veins are magmatic fluids that exsolved from cooling intrusions that assimilated crustal rocks or Belt Supergroup formations. The assimilated crustal rocks may have contributed additional metals and sulfur to intrusions that are genetically related to mineral resources. Galena from the Montana Tunnels breccia pipe is more radiogenic than the base metal vein galena. The increase in  $^{207}\text{Pb}/^{204}\text{Pb}$  and  $^{208}\text{Pb}/^{204}\text{Pb}$  from the Montana Tunnels breccia pipe suggests a different lead isotope source than for the base metal veins or *in situ* radioactive decay of U and Th introduced into the breccia pipe during development.

## INTRODUCTION

Radiogenic lead isotopes are the decay products of uranium and thorium isotopes. The lead isotope  $^{206}\text{Pb}$  is from the decay of  $^{238}\text{U}$ ,  $^{207}\text{Pb}$  is generated from  $^{235}\text{U}$  decay, and  $^{208}\text{Pb}$  is a product of  $^{232}\text{Th}$  decay (Tosdal and others, 1999). The  $^{204}\text{Pb}$  isotope is almost stable and does not decay to another isotope, nor does it have a long-lived parent isotope. The abundance of radiogenic isotopes has grown since the earth formed 4.57 billion years ago, building upon an initial concentration. The measured present day isotope composition is equal to the sum of the initial Pb isotope composition plus radiogenic lead added over time (Tosdal and others, 1999).

Variations in Pb isotopes are impacted by U/Pb and Th/U ratios in the geologic environment over time (Faure, 1977). U and Th have tetravalent oxidation states and can substitute for each other and other high-valence ions in compounds. During partial melting and fractional crystallization, U and Th will concentrate in the liquid phase over the residual phase or crystallized parts of a magma (Tosdal and others, 1999). Thorium has one oxidation state and U has a second oxidation state ( $\text{U}^{6+}$ ), making U soluble and mobile in aqueous fluids. Under oxidizing conditions U forms uranyl ions and will fractionate from Th (Tosdal and others, 1999).

Lead is soluble at moderate to high temperatures found in hydrothermal, magmatic, and metamorphic environments. At low temperatures, lead is generally not soluble but will complex with organic matter (Tosdal and others, 1999). Lead has a larger ionic radius than U and Th, causing it to behave differently during partial melting, metamorphism, and low-temperature alteration events (Tosdal and others, 1999).

Stacey and Kramers (1975) derived a model Pb isotope growth curve from worldwide Pb isotope values. The curve represents the Pb isotope evolution of continental crust based on Pb isotope compositions of galena from ore deposits whose hydrothermal system's Pb isotopes reflected an average of large segments of crust (Tosdal and others, 1999). The average crustal growth curve derived by Stacey and Kramers (1975) is based on two stages of growth characterized by different U/Pb and Th/U ratios. The growth curve provides a reference crustal value to compare Pb isotope compositions measured in rocks and minerals (Tosdal and others, 1999). Deviations of measured Pb isotope values from the average crustal growth curves are caused by geologic events that transport U-Th-Pb from reservoirs with typical crustal values (Tosdal and others, 1999).

Zartman and Haines (1988) used the distinct U/Pb and Th/U characteristics to suggest three idealized crustal reservoirs for U-Th-Pb. These reservoirs are identified to be mantle, lower crust, and upper crust. The three reservoirs mix in the orogene where geologic processes such as magmatism, crustal deformation, metamorphism, and sedimentation take place (Zartman and Haines, 1988). Zartman and Doe (1981) derived model curves for each of the major Pb sources. Lead isotope studies of ore deposits and magmatism relate Pb isotope data to these model reservoirs (Tosdal and others, 1999). Due to geologic events such as partial melting or deformation, Pb isotope data from ore deposits and rocks often deviate from the ideal growth curves (Tosdal and others, 1999). The plumbotectonic model derived by Zartman and Haines (1988) is a broad generalization that is difficult to apply on a local scale. The model does not discriminate between depleted and enriched mantle reservoirs, in part because the role of an enriched reservoir within the mantle was not recognized at the time Zartman and Haines (1988) developed the model (Frances Dudás, written commun., 2018).

Variations in  $^{207}\text{Pb}/^{204}\text{Pb}$  for a whole rock or ore mineral sample is significant for rocks or minerals younger than one billion years (Tosdal and others, 1999). Elevated  $^{207}\text{Pb}/^{204}\text{Pb}$  values indicate regions of the crust where radiogenic Pb evolved in Archean eon rocks because  $^{235}\text{U}$  was more abundant in the Archean (Doe and Zartman, 1979). Elevated  $^{207}\text{Pb}/^{204}\text{Pb}$  further indicates the Pb was not reworked by geologic processes and/or diluted by material with lower  $^{207}\text{Pb}/^{204}\text{Pb}$  values (Tosdal and others, 1999). In contrast, lower  $^{207}\text{Pb}/^{204}\text{Pb}$  values indicate a lack of old radiogenic Pb derived from  $^{235}\text{U}$  decay (Tosdal and others, 1999). The lack of old radiogenic Pb indicates the lead was sourced from an environment such as the mantle that was isolated from old radiogenic crust or derived during recent times from a mantle or oceanic environment (Tosdal and others, 1999).

However, there is a possibility of analytical uncertainty in  $^{207}\text{Pb}/^{204}\text{Pb}$  data showing a smaller range than  $^{206}\text{Pb}/^{204}\text{Pb}$  or  $^{208}\text{Pb}/^{204}\text{Pb}$  data. The analytical uncertainty is caused by the anomalous behavior of  $^{207}\text{Pb}$  during thermal ionization mass spectrometry analysis. Amelin and others (2005) determine even mass isotope ratios follow standard mass fractionation laws, but in contrast, odd to even isotope ratios follow mass-dependent fractionation laws. The differences in fractionation during analysis between odd and even isotopes causes anomalous fractionation of  $^{207}\text{Pb}$  relative to even mass isotopes (Amelin and oth-

ers, 2005). The anomalous fractionation of  $^{207}\text{Pb}$  could lead to analytical uncertainties in some data sets. Due to analytical uncertainties,  $^{207}\text{Pb}/^{204}\text{Pb}$  data need to be cautiously interpreted.

The model lead isotope growth curves derived by Stacey and Kramers (1975), Zartman and Doe (1981), and Zartman (1974) are too general to yield much useful information, but they do provide model ages for potential lead isotope sources. The Pb isotope study of the Stillwater complex by McCallum and others (1999) provides a specific data set for Archean magmatism in Montana and can be used to constrain data sets from other locations in the State. McCallum and others (1999) derived their covariant diagrams from a model crust at 2.7 Ga based on the crustal evolution model of Stacey and Kramers (1975) and the mantle value of 2.7 Ga from the Plumbotectonics IV mantle evolution model of Zartman and Doe (1981). In this study, the covariation diagrams derived by McCallum and others (1999) are used to interpret the lead isotope data along with the model lead isotope growth curves by Stacey and Kramers (1975). Due to the proximity of the Big Belt Mountains to the east of the Boulder Batholith and shared Late Cretaceous ages, Pb isotope data from du Bray and others (2017) were used to further constrain the Boulder Batholith Pb isotope data.

The objectives of this study were to determine the lead isotopic relationships between mineral resources and magmatic events in the Boulder Batholith, identify a magma source for the magmatic events, and identify a metal source for the mineral resources. With the aid of new lead isotope data from 15 mining districts, the Elkhorn Mountains volcanic field, the Lowland Creek volcanic field, intrusions, and lead isotope data from previous investigations, an upper mantle to lower crust source was identified for igneous rocks. Lead isotope data suggest the mineral resources have a genetic relationship with the Boulder Batholith intrusions that may have assimilated upper crust rocks.

Seventeen galena samples from base metal veins and a breccia pipe, and five whole rock samples, were analyzed for  $^{206}\text{Pb}/^{204}\text{Pb}$ ,  $^{207}\text{Pb}/^{204}\text{Pb}$ , and  $^{208}\text{Pb}/^{204}\text{Pb}$  isotope ratios. This data set includes samples from 15 mining districts in the northern half of the Boulder Batholith, three samples from the Elkhorn Mountains volcanic field, one sample from the Lowland Creek volcanic field, and one sample from the Golden Sunlight mine representing a post mineralization diorite dike. This data set was used in conjunction with published Pb-isotope data to interpret the metal source and genesis of Pb in base metal veins and Montana

Tunnels breccia pipe, and identify a magmatic source for the plutons and volcanic rocks.

The study region included the mining districts located in the northern half of the Boulder Batholith and east of the Elkhorn Mountains (fig. 1). These districts were some of the most productive in the Batholith outside the Butte mining district. Previous lead isotope investigations by Dudás and others (2010), Zartman (1992), Zartman and Stacey (1971), Doe and others (1968), Unruh and others (2000), and du Bray and others (2017) covered regions in and near the Boulder Batholith. The previous investigations generated lead isotope data from intrusions, volcanic rocks, and stream sediments throughout the Boulder Batholith and intrusions and mineralized rocks from the Highland Mountains, Little Belt Mountains, and Big Belt Mountains.

## GEOLOGIC SETTING

The Late Cretaceous Boulder Batholith (fig. 1) covers an area of 2,200 mi<sup>2</sup> and intruded Precambrian to Late Cretaceous rocks of diverse lithology (Doe and others, 1968). The Batholith is in the Great Falls Tectonic Zone within the fold-thrust belt of southwestern Montana. The collision of Archean and Paleoproterozoic terrane about 1,800 mega-annum (Ma) created the Great Falls Tectonic Zone. A north-west-trending depositional trough known as the Belt Basin formed approximately 1,500 Ma and crosses the Great Falls Tectonic Zone. Proterozoic northwest-striking faults forming the Lewis and Clark Line are exposed in the west-central and southeast part of the Belt Basin (Berger and others, 2011).

Magmatic and tectonic activity took place in western Montana during the Laramide orogeny (Late Cretaceous to Eocene; Berger and others, 2011). Magma moved into the crust during the Laramide orogeny between about 85 and 65 Ma and Mississippian–Cretaceous sedimentary rocks were regionally shortened and deformed, developing the fold-thrust belt (Robinson and others, 1968; Kalakay and others, 2001; Lageson and others, 2001; Lund and others, 2007). Concurrent left-lateral transpression along the Lewis and Clark Line cuts the Cordilleran fold-thrust belt. Middle Proterozoic Belt Supergroup formations were juxtaposed by fold-thrust belt tectonism (Sears and others, 2010).

The Elkhorn Mountains volcanic field (EMVF) and Boulder Batholith formed concurrently during crustal shortening near the end of Mesozoic Cordillera arc magmatism between about 85 and 76 Ma (Mahoney and others, 2015; Rutland and others, 1989). The

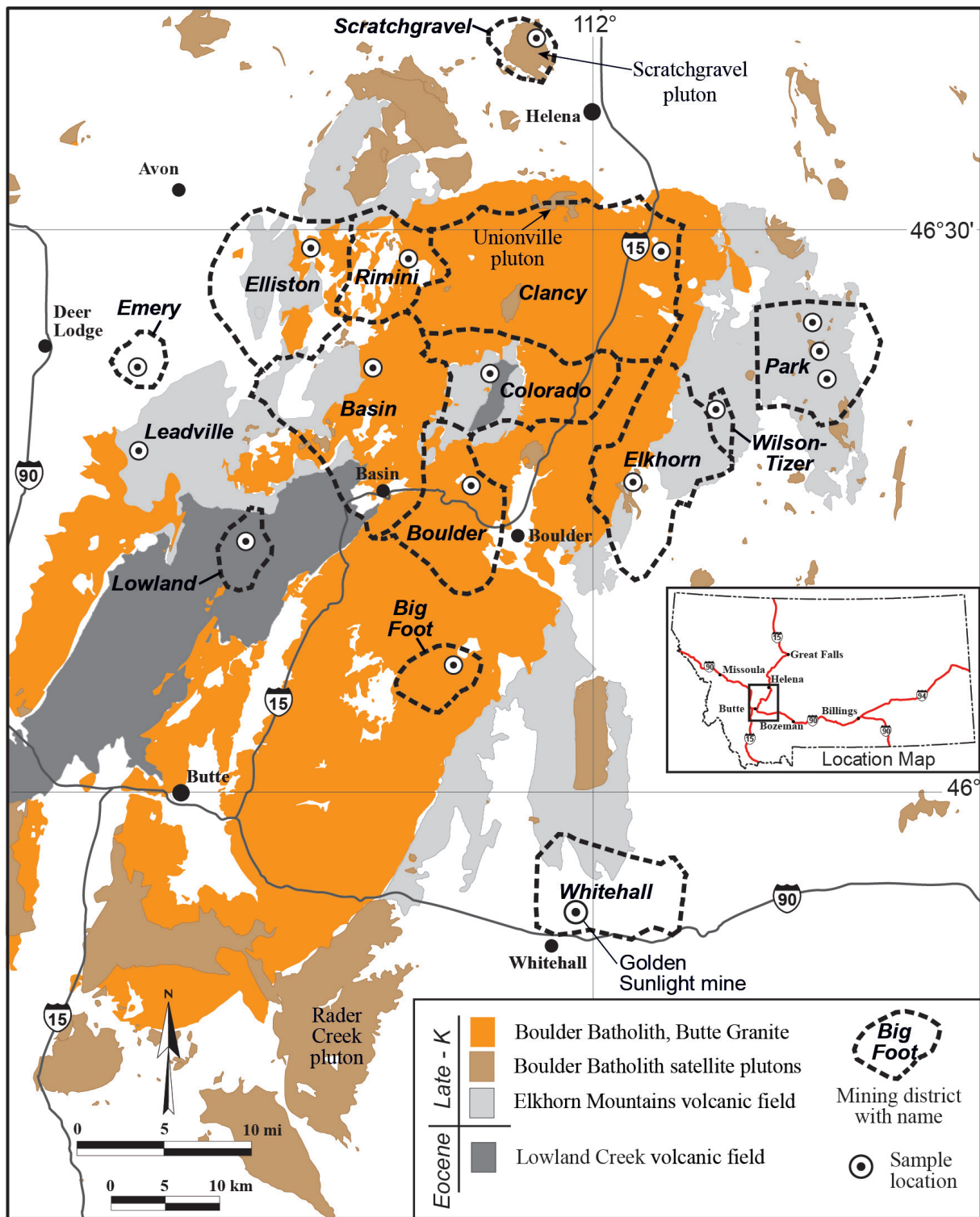


Figure 1. Geologic map of Boulder Batholith showing mining districts and approximate locations for base metal vein galena samples.

EMVF is preserved along the west and east flanks of the Boulder Batholith (fig. 1) and was the first magmatic event during continental arc magmatism in the region. Intruded into the EMVF and Mesoproterozoic to Mesozoic sedimentary rocks are the Boulder Batholith or Butte Granite and a group of associated smaller plutons (du Bray and others, 2012).

Magmatic events that developed the Boulder Batholith started at the same time as the EMVF eruption. Field relationships indicate the Batholith was emplaced into the EMVF between 85 and 76 Ma (Tilling and others, 1968; Mahoney and others, 2015). A 950-m section of EMVF ignimbrites south of Boulder, Montana has an  $^{40}\text{Ar}/^{39}\text{Ar}$  age ranging from  $83.7 \pm 0.3$  to

84.9 ± 2.6 Ma (Olson and others, 2016). The Boulder Batholith plutons and Butte Granite were emplaced from 81.7 ± 1.4 Ma to 73.7 ± 0.6 Ma (du Bray and others, 2012). The Butte Granite is the main pluton by volume of the Boulder Batholith, and U/Pb zircon ages are 74.5 ± 0.9 Ma (Lund and others, 2002) and 76.28 ± 0.14 Ma (Martin and others, 1999). The Butte Granite could be a composite formed from two episodes of magmatism (du Bray and others, 2012).

Intrusion of pegmatite, alaskite, and aplite dikes took place at the close of Butte Granite magmatism (Berger and others, 2011). The dikes have a north-east orientation and are found in a northeast-trending, 4- to 6-km-wide zone extending across the Batholith. After the Butte Granite and dikes crystallized, sulfide-bearing quartz veins with an east–west orientation developed in the northern half of the Batholith (Berger and others, 2011). Olson and others (2016) determined <sup>40</sup>Ar/<sup>39</sup>Ar plateau ages for two veins in the Big Foot district. A vein at the State mine was determined to be 75.2 ± 0.25 Ma (95% confidence) and a <sup>40</sup>Ar/<sup>39</sup>Ar plateau age for the vein at the Ajax mine to be 73.81 ± 0.12 Ma (95% confidence). The ages of the veins are about a million years younger than the host Butte Granite.

Eocene crustal extension and Basin and Range faulting caused the EMVF and Boulder Batholith to be uplifted, eroded, and exhumed. Laramide crustal shortening about 65–55 Ma followed by extension formed grabens in the upper plate of the Anaconda Metamorphic Core Complex detachment. The Lowland Creek volcanic field (LCVF) erupted between 53 and 49 Ma during crustal extension, filling a north-east–southwest-trending half graben traversing the Boulder Batholith (Sillitoe and others, 1985; Scarberry and others, 2015; Dudás and others, 2010; fig. 1). The Lowland Creek volcanic rocks overlie the Elkhorn Mountains volcanic rocks and the Butte Granite. Underlying the LCVF near the western end of the graben are Mid-Proterozoic, Permian, and Cretaceous sedimentary rocks (Dudás and others, 2010). The LCVF hosts the Montana Tunnels and Tuxedo mine breccia pipes or diatremes (Sillitoe and others, 1985; Lawson and others, 1937).

Extension-related core complex formation continued during and after Lowland Creek volcanism until about 35 Ma (Lonn and Elliott, 2010). Near the close of Lowland Creek volcanism, basin sedimentation began (Portner and others, 2011). Overlying the LCVF are lacustrine and fluvial sedimentary rocks in the Deer Lodge and Warm Springs Creek Valleys, which are locally unconformable above the volcanic rocks (Dudás and others, 2010).

Compositions of the plutons making up the Boulder Batholith are similar to those of moderately differentiated subduction-related magmas (du Bray and others, 2012). Compositions vary from subalkaline, magnesian, calcic-alkalic to calcic and metaluminous to peraluminous (du Bray and others, 2012). du Bray and others (2012) report the major oxide abundances of the Butte Granite intrusion are homogeneous. The satellite plutons are characterized by distinct trace element abundances, but these trace element abundance variations are minor. Even though the Boulder Batholith hosts significant mineral deposits, ore metal abundances in the Butte Granite and satellite plutons are not elevated and are comparable to global average abundances in igneous rocks (du Bray and others, 2012).

## PREVIOUS INVESTIGATIONS

The first lead isotope study on the Boulder Batholith including the Butte mining district was done by Murthy and Patterson (1961). They suggested the ore metals came from multiple sources that were transported into the Batholith by late-stage magmatic fluids after the Batholith was intruded. They proposed ore mineral and host rock lead isotopes were mixed in and near the ore zone. The hypothesis presented by Murthy and Patterson (1961) contradicted the vein genesis hypothesis of Grunig and others (1961). Grunig and others (1961) disputed Murthy and Patterson's (1961) hypothesis by providing evidence the Butte ores were derived from the differentiation and concentration of a late-stage fluid with a magmatic origin and not from multiple outside sources.

Doe and others (1968) published the results of a lead and strontium isotope study on the Boulder Batholith that included satellite plutons, volcanic rocks, and Butte Granite. They determined a Precambrian age for the lead source and discussed three possible models for the origin of the plutons and volcanic rocks. Doe and others (1968) concluded the plutons and volcanic rocks originated from partial melting of lower crustal and/or mantle material and, in some plutons, Precambrian Belt and pre-Belt rocks were assimilated into the melts.

Lead isotopes and mineralization ages for sulfide veins hosted by Belt Supergroup rocks in northwestern Montana and northern Idaho were investigated by Zartman and Stacey (1971). They used contrasting lead isotope populations to distinguish between Precambrian and Mesozoic or Cenozoic mineralization. Zartman and Stacey (1971) concluded Precambrian veins have a uniform lead isotope composition that is

the product of single-stage development. They identified the possibility that vein deposits that formed at a later time incorporated lead remobilization from Belt rocks. Zartman and Stacey (1971) noted Mesozoic and Cenozoic vein deposits have more radiogenic lead and wider isotopic compositions than Precambrian veins, reflecting two-stage development.

Zartman (1974) identified three lead isotope provinces in the Cordillera of the western United States that includes western Montana. The provinces Zartman (1974) identified reflect the geology of the source rocks from which the lead was acquired. The three provinces are designated as area I, area II, and area III. In area I, lead is sourced principally from Precambrian crystalline basement. Area II lead isotopes are sourced from sedimentary rocks eroded from Precambrian rocks, and area III contains lead derived from eugeosynclinal plutonic, volcanic, and sedimentary rocks forming a belt adjacent to the Pacific coast. Western Montana is located in lead isotopic province area I, suggesting lead sourced from Precambrian crystalline basement rocks.

A lead isotope study on the Helena embayment by Zartman (1992) included Belt rocks exposed in the Highland Mountains, Little Belt Mountains, Bridger Range, and Belt rock hosted sulfide veins. Zartman (1992) found two lead isotope populations for galena hosted by Middle Proterozoic Belt Supergroup rocks. Most of the Belt Basin is characterized by uniform isotopic compositions with minor variability in isotope ratios. Zartman (1992) attributed the minor variability of more radiogenic isotope ratios to remobilization of the original stratabound sediments and mixing between marine and continental sediments. Zartman (1992) found a distinctive Archean lead isotope signature for the Helena embayment, suggesting an Archean crystalline sedimentary source for Belt rocks. However, only the LaHood Formation had an isotopic signature related to an Archean provenance; lead isotopes from the other formations had a marine provenance (Zartman, 1992).

The Lowland Creek volcanic field was investigated for lead isotopes and  $^{40}\text{Ar}/^{39}\text{Ar}$  geochronology by Dudás and others (2010). The investigation included an andesite sample from the Elkhorn Mountain volcanic field near the Emery mining district and a Boulder Batholith related intrusion near Mill Creek. They identified four different  $^{206}\text{Pb}/^{204}\text{Pb}$  components representing different Lowland Creek volcanic eruptions and rock types. The first three lead isotope components were probably derived from a lower to middle crustal source. The fourth lead isotope component,

represented by andesite, was probably derived from a lithospheric mantle source.

Lead isotopic data and element concentrations of streambed sediments from Basin Creek, Cataract Creek, and High Ore Creek in the Basin mining district were determined by Unruh and others (2000). The purpose of their study was to determine the pre-mining trace element concentrations in streambed sediments to be used as a baseline to determine the impact of mining on the Boulder River. Samples were taken upstream from historic mining activity, stream terrace deposits located upstream and downstream of the major tributaries of the Boulder River, and sediment cores from over bank deposits, abandoned stream channels, or beneath fluvial mill tailings deposits. They reported on lead isotope data for 6 stream-terrace samples and 13 sediment core samples.

Isotopic data were generated by du Bray and others (2017) for the Big Belt Mountains located east of the Boulder Batholith. They used O, Nd, Sr, Rb, Sm, and Pb isotopes to identify the petrogenesis of the Mount Edith and Boulder Baldy intrusions. From the isotopic study, a combination of compositionally heterogeneous sources was identified as having variable isotopic contamination from crustal assimilation (du Bray and others, 2017). Altered and mineralized rocks related to the intrusions demonstrate two isotopically distinct mineralizing events involving major inputs from associated Late Cretaceous igneous rocks (du Bray and others, 2017). The isotopic source for the mineralizing events identified by du Bray and others (2017) was fluids that equilibrated with Newland Formation quartzite. They found oxygen isotopes for the Boulder Baldy intrusive to be similar to those of subduction-related magmatism that included mantle-derived components.

## ANALYTICAL PROCEDURES

Isotopic compositions of Pb in whole-rock and galena samples were determined at the USGS Crustal Geophysics and Geochemistry Science Center, Radiogenic Isotope Laboratory in Denver, Colorado. Seventeen galena samples representing base metal veins from 15 mining districts and 5 whole rock samples were submitted for analysis. Samples representing vein sections were collected from mine dumps and whole rock samples were collected from outcrops. Slabs were cut from vein section samples to expose the sulfide minerals and embedded galena grains. Some slabs were coarsely crushed to aid in separating disseminated galena grains from unwanted sulfides and quartz. Galena grains were handpicked

from cut slabs and crushed samples under a binocular microscope. Whole rock samples were powdered samples used for previous ICP-MS analysis determined at the Washington State University, Peter Hooper Geo Analytical Laboratory, School of the Environment, Pullman, Washington.

Lead was separated from whole rock samples for isotope analysis on AG1-X8 resin columns in HBr medium. The Pb analyses was conducted by isotope dilution, thermal-ionization, mass spectrometry (ID TIMS). Splits of powdered whole rock were digested over 3 days on a hot plate at 135°C using a mixture of HNO<sub>3</sub> and HF with <sup>205</sup>Pb spike solution. The total procedural Pb blank for whole rock analysis was ≈10 picograms and the whole rock data were corrected for the blank and spike contribution. No Pb blank correction was necessary for the galena analyses, which were conducted on un-spiked digested mineral without chemical separation of Pb.

The isotopic analysis was conducted using a multi-collector TIMS Triton. Isotope ratios were measured in static mode using Faraday cups. Measured Pb-isotope ratios were corrected for mass fractionation of 0.0007 ± 0.0003 per mass unit using raw data for NIST Pb isotope standard SRM-981 measured at the same run conditions. Correction factors for Pb

isotope data based on multiple runs of NIST standard SRM-981 is shown in appendix A.

## RESULTS

Lead isotope compositions from base metal vein galena, breccia pipe galena, and whole rock samples are shown in appendix A. New analytical results (appendix A) and previous data are plotted on covariant diagrams figures 2–15. Analytical results are given in atomic percent ratios relative to <sup>204</sup>Pb with analytical errors of ± 0.014 to ± 0.018 for <sup>206</sup>Pb/<sup>204</sup>Pb, ± 0.02 to ± 0.023 for <sup>207</sup>Pb/<sup>204</sup>Pb, and ± 0.061 to ± 0.065 for <sup>208</sup>Pb/<sup>204</sup>Pb. The lead isotope data for the base metal vein galena, volcanic, and intrusive rocks is relatively consistent with little variation. The galena sample from the Montana Tunnels breccia pipe was more radiogenic than the galena samples from the base metal veins, volcanic rocks, and intrusions. The results are similar to those of past investigations with little variation (appendices B–F).

The lead isotope data from the base metal veins plotted on covariant diagrams overprints data from previous intrusive rock investigations. The overprinting of the base metal veins and intrusion Pb isotopes constrains the Pb isotopes to a single source and constrains vein development to hydrothermal fluids with a

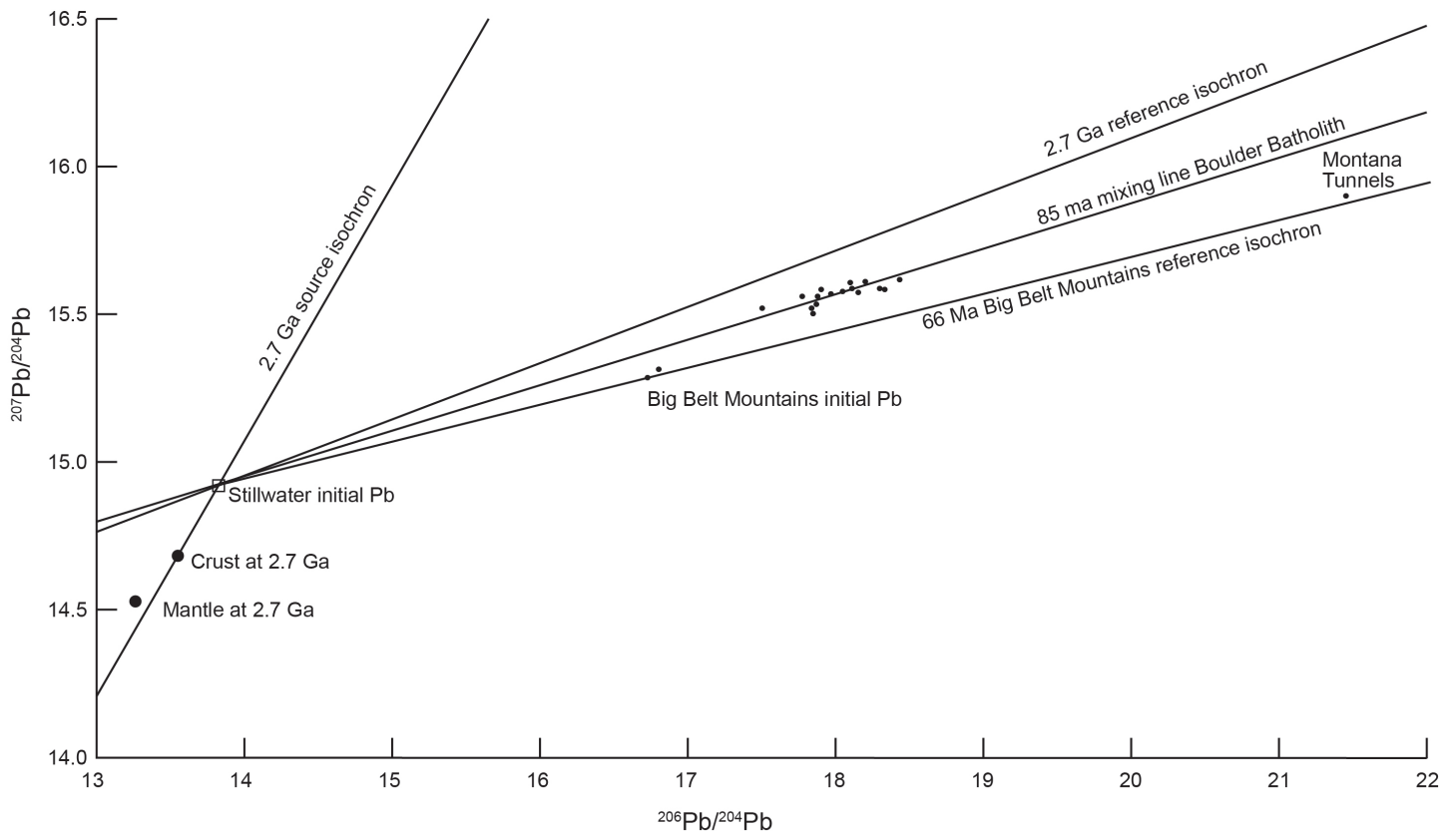


Figure 2. Covariant diagram of <sup>206</sup>Pb/<sup>204</sup>Pb vs. <sup>207</sup>Pb/<sup>204</sup>Pb plot for base metal vein and breccia pipe galena lead isotope ratios generated by this investigation. MT, Montana Tunnels data point.

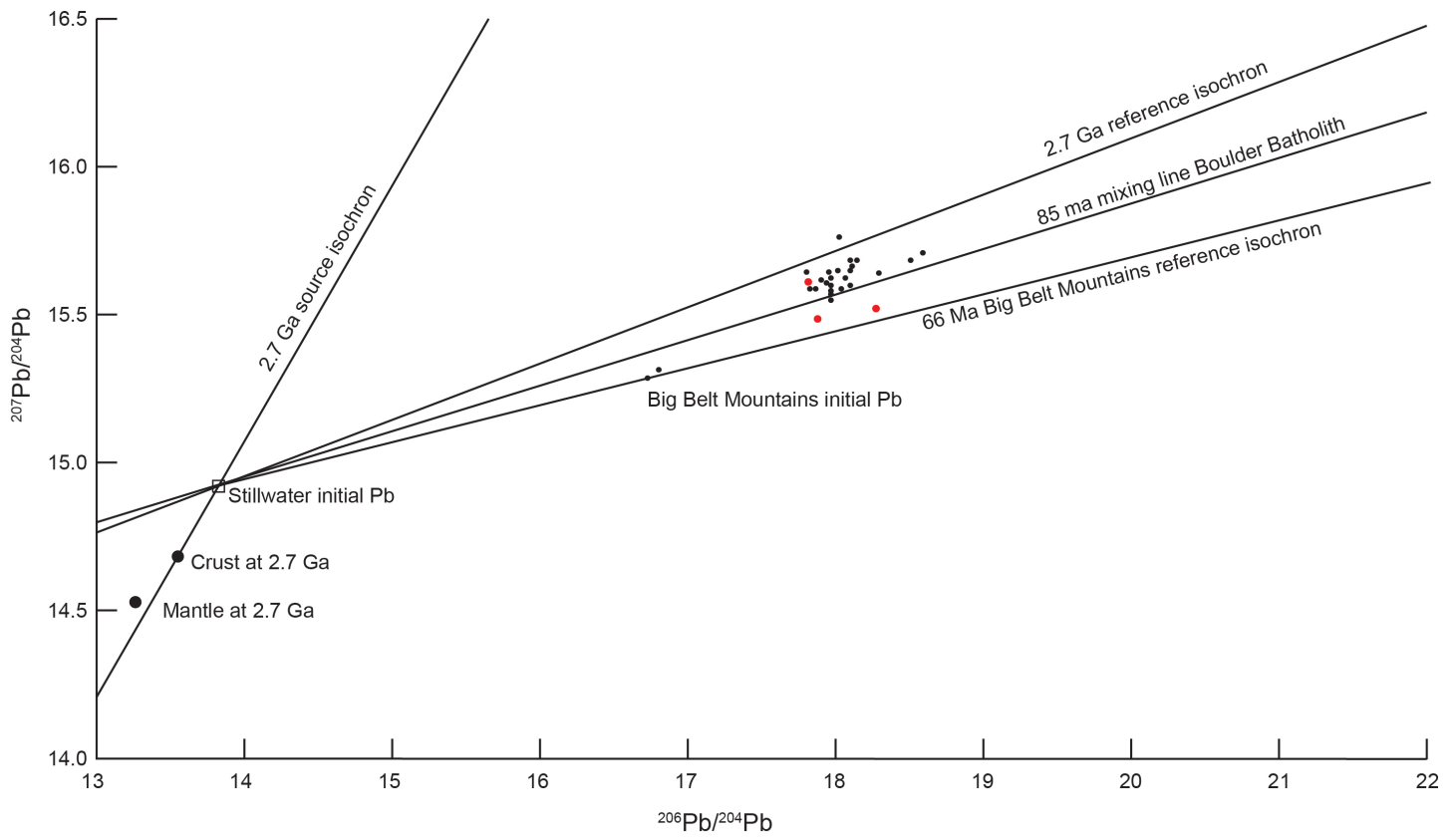


Figure 3. Covariant diagram of  $^{206}\text{Pb}/^{204}\text{Pb}$  vs.  $^{207}\text{Pb}/^{204}\text{Pb}$  plot for Boulder Batholith intrusions published by Doe and others (1968) with added data generated by this investigation (red points).

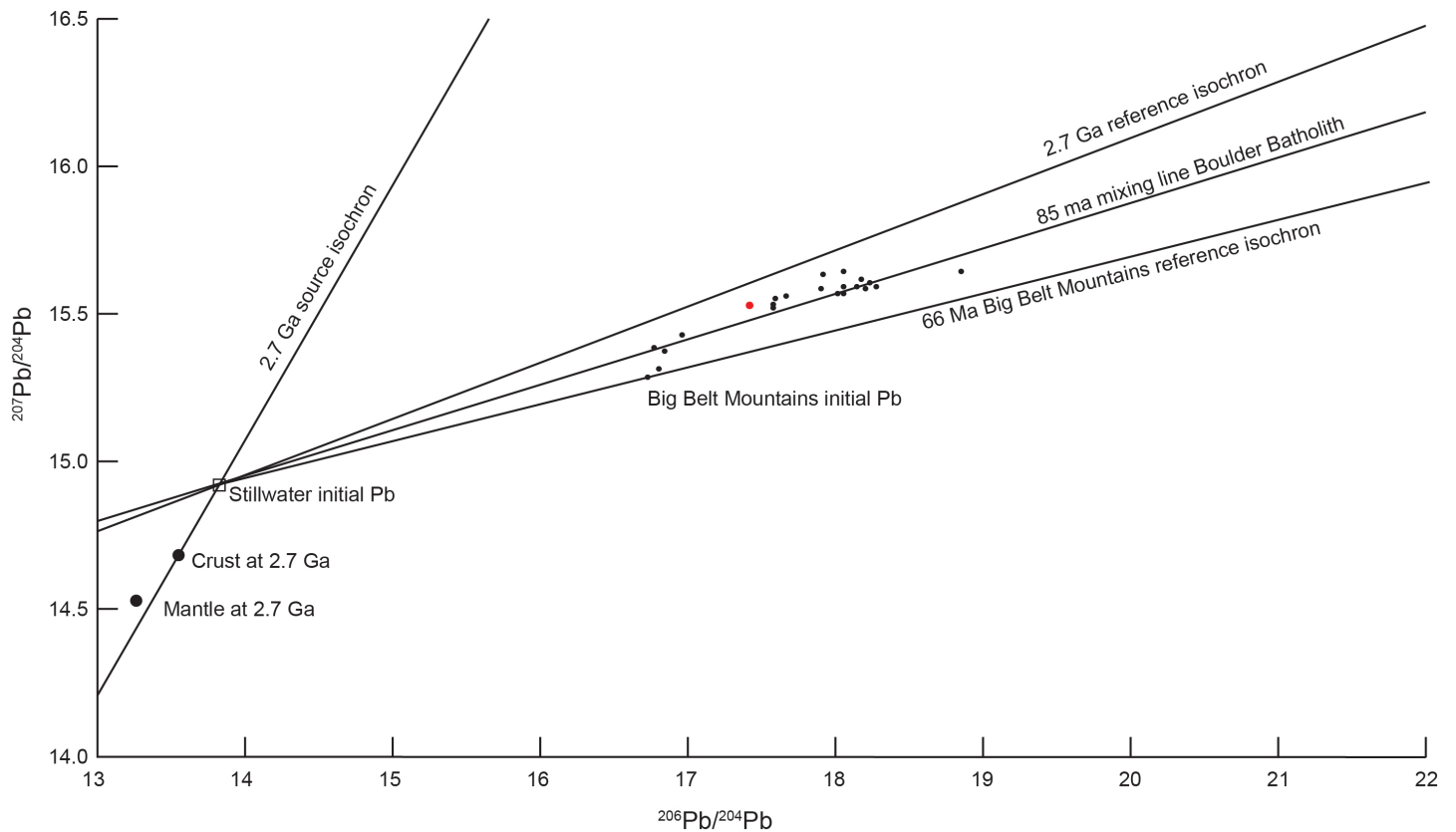


Figure 4. Covariant diagram of  $^{206}\text{Pb}/^{204}\text{Pb}$  vs.  $^{207}\text{Pb}/^{204}\text{Pb}$  plot for Lowland Creek volcanic rocks published by Dudás and others (2010) with added data generated by this investigation (red point).

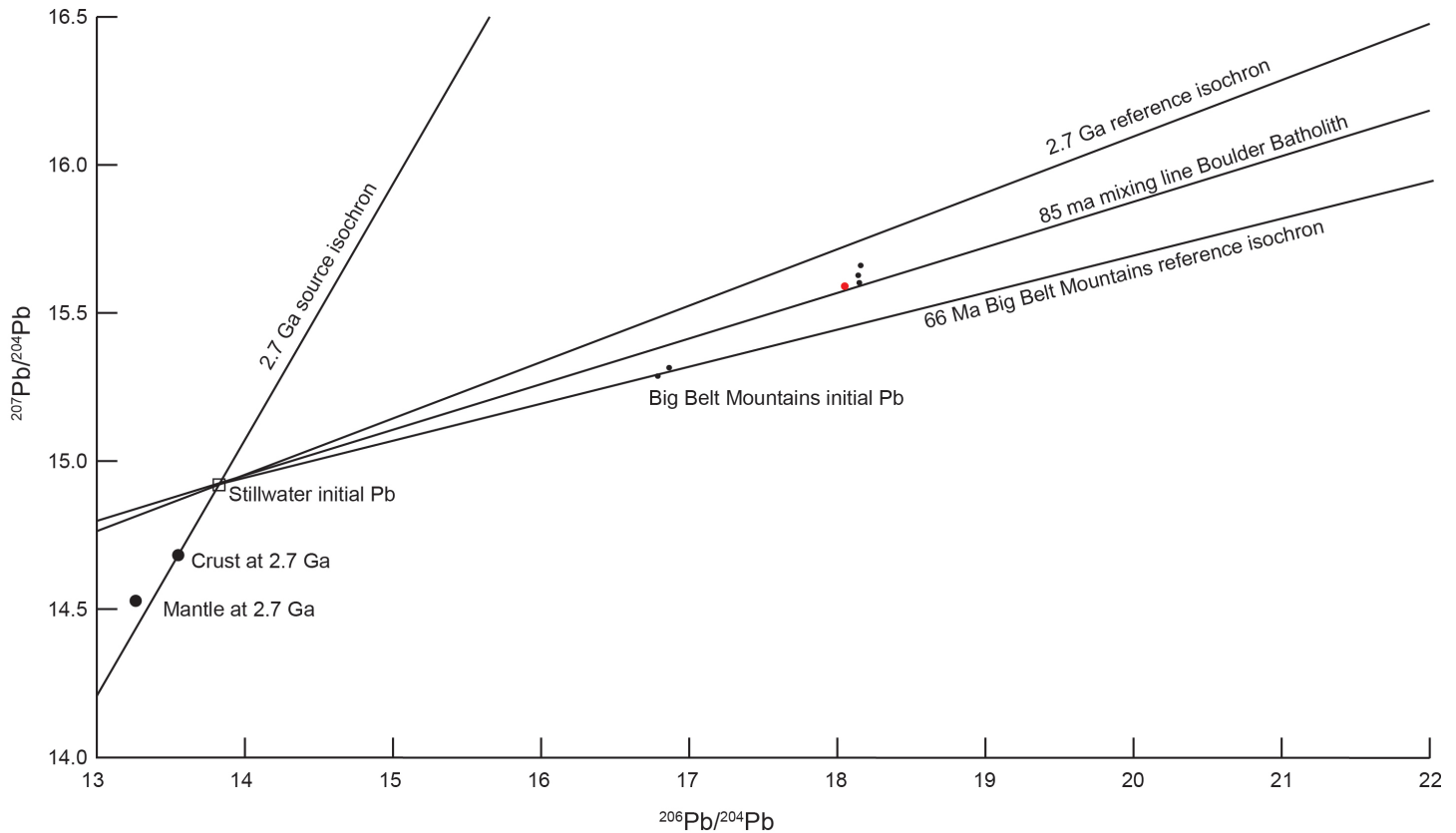


Figure 5. Covariant diagram of  $^{206}\text{Pb}/^{204}\text{Pb}$  vs.  $^{207}\text{Pb}/^{204}\text{Pb}$  plot for Elkhorn Mountains volcanic rocks published by Doe and others (1968) with added data generated by this investigation (red point).

magmatic source. These constraints restrict the timing of mineralization and vein development to intrusive and volcanic events. The more radiogenic Montana Tunnels galena sample might have been influenced by the process that formed the breccia pipe or represent a different lead isotope source than the base metal veins. *In situ* radiogenic decay of uranium and thorium transported into the breccia pipe from an outside source during mineralization may have increased the concentration of radiogenic lead.

Lead isotope results from this investigation and past investigations are plotted on  $^{206}\text{Pb}/^{204}\text{Pb}$  vs.  $^{207}\text{Pb}/^{204}\text{Pb}$  covariant diagrams (figs. 2–15). On the diagrams, the line labeled 2.7 Ga source isochron and 2.7 Ga reference isochron are from McCallum and others (1999). The line labeled 66 Ma Big Belt Mountains reference isochron is based on the least radiogenic sample from the Boulder Baldy intrusion core (du Bray and others, 2017) and is constrained by the Stillwater initial Pb isotope value. The line labeled 85 Ma mixing line Boulder Batholith is based on a point cluster average for all samples of the Boulder Batholith and is constrained by the Stillwater initial Pb isotope value.

## DISCUSSION

Western Montana is dominated by Archean and Proterozoic crust that may have been an initial source for lead isotopes found in the veins and intrusions of the Boulder Batholith. Zartman (1974) identified three lead isotopic provinces based on lead isotope compositions from volcanic and plutonic rocks in the western United States. Crustal lead isotopes found in western Montana are principally derived from the Precambrian crystalline basement (Zartman, 1974). Average lead isotopic data from Zartman (1974) suggest western Montana is underlain by 2.7 Ga basement rocks.

Data from the Stillwater J-M reef sulfides published by McCallum and others (1999) can provide a lead isotope baseline for the 2.7 Ga Archean rocks in Montana. Covariant plots for the 2.7 Ga initial lead isotope data for Stillwater was used to constrain the lead isotope data from this investigation of the Boulder Batholith along with data comparisons from previous investigations. Lead isotope data determined by du Bray and others (2017) from the Big Belt Mountains was used to further constrain the Boulder Batholith data. Lead isotope data from past investigations by Doe and others (1968), Zartman (1992), Unruh and others (2000), Dudàs and others (2010), and du Bray

and others (2017) were used to compare and constrain data from this investigation and are summarized in appendices B–F.

Lead isotope data from this investigation and past investigations are plotted on a  $^{206}\text{Pb}/^{204}\text{Pb}$  vs.  $^{207}\text{Pb}/^{204}\text{Pb}$  covariant Pb isotope diagrams (figs. 2–8) based on the Stillwater investigation by McCallum and others (1999). The line on the plot from McCallum and others (1999) labeled 2.7 Ga source isochron represents a range of source compositions based on Stacey and Kramers (1975) parameters at 3.7 Ga and evolution to 2.7 Ga with a variable  $\mu(^{238}\text{U}/^{204}\text{Pb})$ . This line serves as a reference for possible lead isotope compositions sourced from Archean rocks in western Montana. Lead isotopic ratios that plot along the source isochron line were not influenced by outside geologic processes such as intrusive and metamorphic events causing additions and/or subtractions of Pb isotopes and were directly sourced from the crust. The source isochron line constrained by the Stillwater initial Pb ratios passes through the model crust value but not the model mantle value. The 2.7 Ga reference isochron line is constrained to pass through the Stillwater initial Pb isotopic composition (McCallum and others, 1999).

Lead isotope ratios plotted on the  $^{206}\text{Pb}/^{204}\text{Pb}$  vs.  $^{207}\text{Pb}/^{204}\text{Pb}$  covariant diagram (figs. 2–7) shows a clustering of points below the 2.7 Ga source isochron reference line. Lead isotope data from past investigations and this investigation are similar and overlap following similar trends on the covariant diagrams. These similarities between the different data sets imply they share a similar isotopic source. Plotting below the 2.7 Ga reference isochron suggests the isotopic compositions were influenced by mixing between 2.7 Ga crustal lead and less radiogenic sources. An exception can be found for the Proterozoic Belt Supergroup formations and sulfide veins (fig. 8); these Pb isotopes plot above the 2.7 Ga reference line. Lead isotopes plotting above the 2.7 Ga reference isochron imply an Archean crustal influence for the Proterozoic Belt Supergroup formations and sulfide veins.

A mixing line for the Boulder Batholith constrained to pass through the Stillwater initial isotopic composition was drawn through the point cluster for all the Boulder Batholith data and represents the addition of externally derived lead isotopes. The Boulder Batholith mixing line suggests lead isotopes sourced from Archean crust was influenced by geologic processes adding additional radiogenic isotopes to the magmas that generated the plutons and volcanic rocks. This

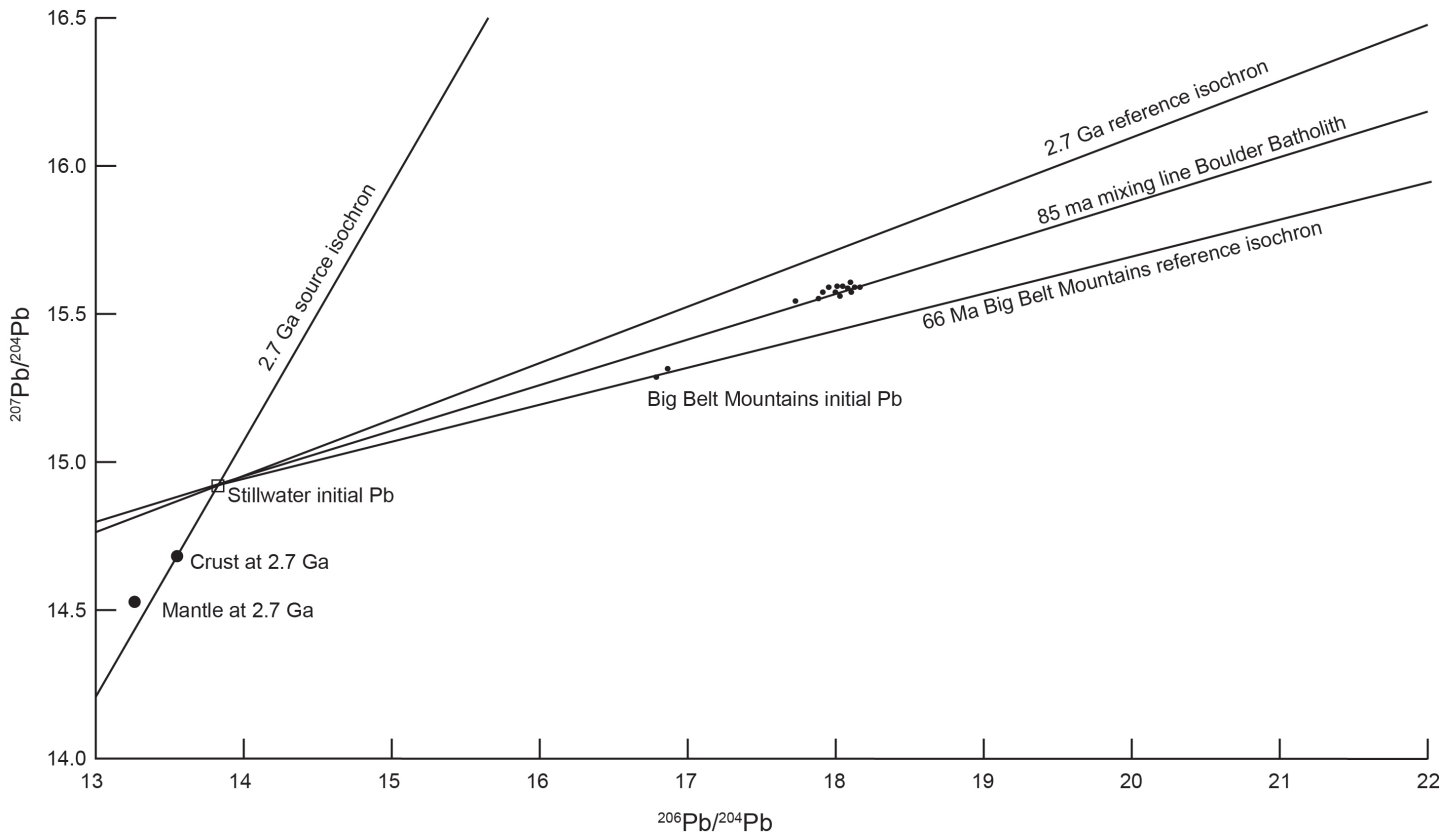


Figure 6. Covariant diagram of  $^{206}\text{Pb}/^{204}\text{Pb}$  vs.  $^{207}\text{Pb}/^{204}\text{Pb}$  plot for Basin Mining district stream sediment samples published by Uhrh and others (2000).

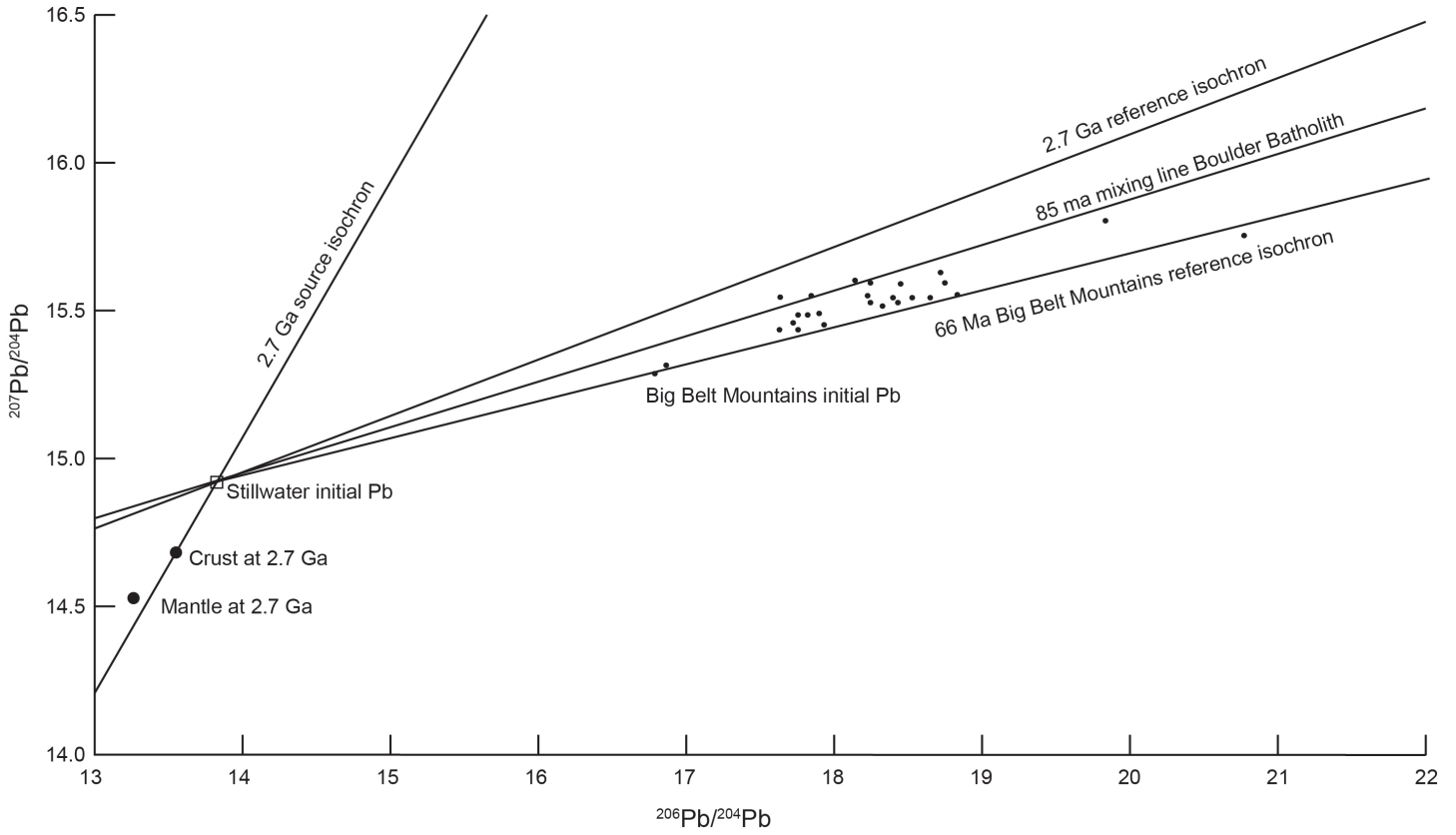


Figure 7. Covariant diagram of  $^{206}\text{Pb}/^{204}\text{Pb}$  vs.  $^{207}\text{Pb}/^{204}\text{Pb}$  plot for the Big Belt Mountains published by du Bray and others (2017).

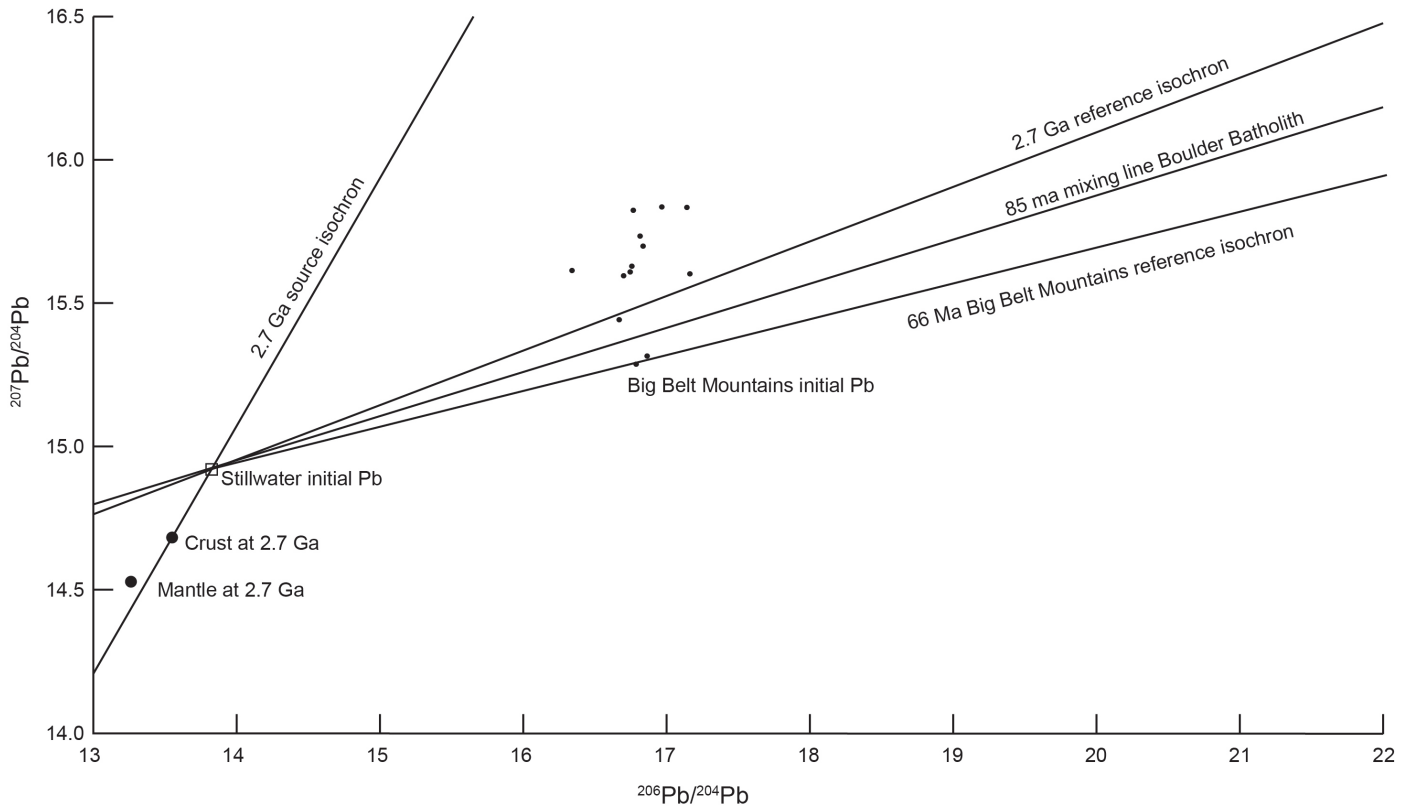


Figure 8. Covariant diagram of  $^{206}\text{Pb}/^{204}\text{Pb}$  vs.  $^{207}\text{Pb}/^{204}\text{Pb}$  plot for the Belt Supergroup formations and sulfide veins published by Zartman (1992).

mixing of Pb isotopes took place at the beginning of the Laramide orogeny about 85 Ma when subduction zone magmas were being generated and continued until the close of magmatic and mineralizing events.

The age (68 to 66 Ma) and proximity of the Big Belt Mountains to the Boulder Batholith imply they were developed from the same geologic process during the Laramide orogeny. Due to this geologic and age relationship, the Big Belt Mountains will be used as a reference for constraining Pb isotope compositions from the Boulder Batholith. In figures 2 to 8, the Big Belt Mountains reference isochron was drawn using the least radiogenic sample from the core of the Boulder Baldy intrusion and constrained through the Stillwater initial Pb isotope reference point. The isochron age is based on the 66.2 Ma U-Pb age for zircon from the intermediate zone of the intrusion (du Bray and others, 2017). Petrogenesis of the Boulder Baldy intrusion core involved Archean to Proterozoic mafic to intermediate basement-derived magma (du Bray and others, 2017). Lead isotope data that plot on or near the Big Belt Mountains reference line have a greater subcontinental lithospheric-derived component than those that plot above the line, which have a greater crustal-derived contamination. Lead isotopic data constrained between the 2.7 Ga reference isochron and the 66 Ma Big Belt Mountains isochron will have greater Archean to Proterozoic crustal-derived contamination with more radiogenic Pb isotopes than those plotting on or near the 66 Ma Big Belt Mountains isochron.

The covariant  $^{208}\text{Pb}/^{204}\text{Pb}$  vs.  $^{206}\text{Pb}/^{204}\text{Pb}$  diagram based on the Stillwater investigation by McCallum and others (1999) was used to constrain the lead isotope data from this investigation and past investigations (figs. 9–15). The 2.7 Ga source isochron represents the range of possible model crust lead isotope values sourced from the Archean crust. McCallum and others (1999) constructed the line based on Stacey-Kramers model values using a Th/U value of 3.8 and a variable  $\mu_o$ . The 2.7 Ga source isochron is constrained to pass through the Stillwater initial lead isotope value (McCallum and others, 1999). Lead isotopes that plot close or below the 2.7 Ga source isochron are undisturbed, possibly originating from a mantle-derived magma (McCallum and others, 1999). Lead isotopes plotting above the model crust values of the 2.7 Ga source isochron will most likely originate from crustal- or mantle-derived magmas contaminated with the addition of radiogenic crust. A 2.7 Ga reference isochron constrained to pass through the Stillwater initial lead value, calculated for Th/U = 3.8, from Mc-

Callum and others (1999), was added to the covariant diagrams. Lead isotopes that plot on or below the 2.7 Ga reference line could originate from a crustal- or mantle-derived magma contaminated with additional radiogenic crust.

A 66 Ma Big Belt Mountains reference isochron was plotted using the least radiogenic sample from the Boulder Baldy intrusion core and age of the intermediate zone (du Bray and others, 2017) and constrained to pass through the Stillwater initial lead isotope value (figs. 9–15). Lead isotopes that plot on or near the Big Belt Mountains reference isochron contain a higher subcontinental lithospheric lead isotope component than lead isotopes that plot below the line, which was influenced by crustal assimilation.

A mixing line was constructed for the Boulder Batholith passing through the cluster of points and constrained by the Stillwater initial Pb isotope composition (figs. 9–15). Most lead isotope data for the Boulder Batholith is constrained between the 66 Ma Big Belt Mountains reference isochron and the 2.7 Ga reference isochron (figs. 9–13) and cluster around the 85 Ma mixing line. The constraint of the Boulder Batholith lead isotopes shown on figures 9–13 suggest they are more radiogenic than the 2.7 Ga model crust. This implies that the lead isotope compositions were influenced by the addition of radiogenic lead from an outside source or *in situ* radioactive decay.

Lead isotope mixing lines for plutons in the Boulder Batholith was proposed by Doe and others (1968). The mixing lines on  $^{206}\text{Pb}/^{204}\text{Pb}$  vs.  $^{207}\text{Pb}/^{204}\text{Pb}$  and  $^{206}\text{Pb}/^{204}\text{Pb}$  vs.  $^{208}\text{Pb}/^{204}\text{Pb}$  covariant diagrams by Doe and others (1968) are similar to the mixing lines proposed for this investigation shown in figures 2–15. Lead isotope mixing lines have likewise been identified by du Bray and others (2017) for the Big Belt Mountains intrusions located on the northeast edge of the Boulder Batholith. The mixing lines (figs. 2–6 and 9–13) for the veins, intrusions, and volcanic rocks of the Boulder Batholith suggest the initial magma source was contaminated with the addition of radiogenic crust during intrusive events. The single mixing lines on figures 2–6 and 9–13 suggest the veins were mineralized during single events related to different magmatic intrusions that started with the eruption of the Elkhorn Mountains volcanic field and ended with the eruption of the Lowland Creek volcanic field.

To further differentiate between lead isotope sources, data were plotted on model lead growth curves from Stacey and Kramers (1975; figs. 16–22). The ages on the model lead growth curves are model ages and do not reflect the Boulder Batholith 85 Ma

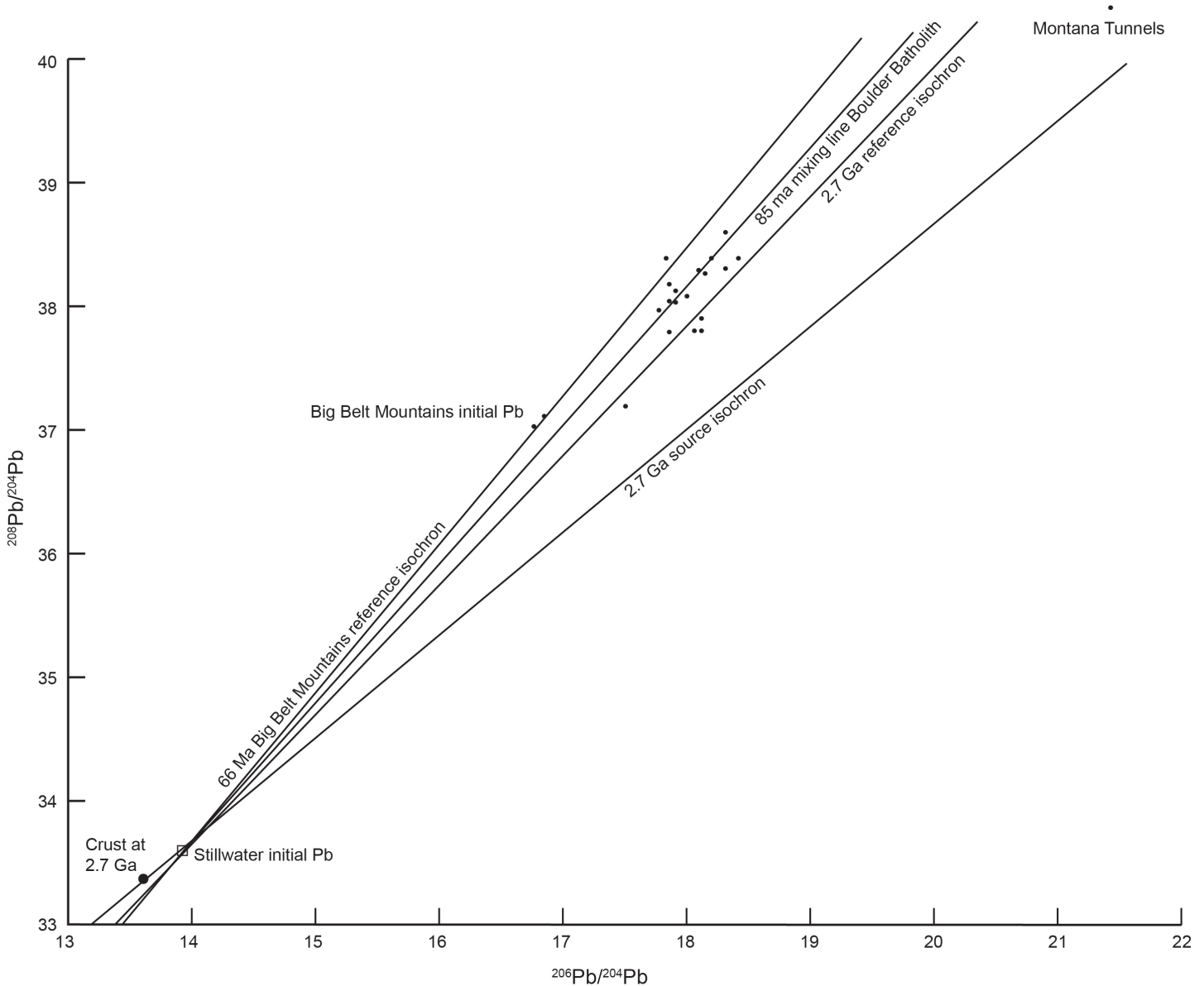


Figure 9. Covariant diagram for  $^{208}\text{Pb}/^{204}\text{Pb}$  vs.  $^{206}\text{Pb}/^{204}\text{Pb}$  plot for base metal vein and breccia pipe galena lead isotope data generated by this investigation.

to 45 Ma ages for the veins or intrusions. The model ages on the lead growth curves are related to the lead isotope source ages. Lead isotopes from the base metal veins, intrusions, and volcanic rocks have similar lead isotope compositions with overlapping ranges (table 1). Plotted on covariant diagrams and model lead growth curves (figs. 2–6, 9–13, and 16–21), lead isotopes from the intrusions, stream sediments, base metal veins, and volcanic rocks overlap along mixing lines and model lead growth curves. This suggests a common origin between vein mineralization and intrusive events.

### Base Metal Veins

The base metal veins plotted on  $^{206}\text{Pb}/^{204}\text{Pb}$  vs.  $^{207}\text{Pb}/^{204}\text{Pb}$  covariant diagram (fig. 2) show little deviation from the mixing line. On the  $^{206}\text{Pb}/^{204}\text{Pb}$  vs.  $^{208}\text{Pb}/^{204}\text{Pb}$  diagram (fig. 9), the Pb isotope data show a wide deviation from the mixing line. The inconsistencies between the two covariant diagrams (figs. 2 and 9) suggest a heterogeneous isotope source for the base metal veins. On the model lead growth curves (fig. 16), model ages vary from 800 Ma to 200 Ma, suggesting a variety of isotope sources during vein development. Vein mineralization took place from about 74 Ma to 45 Ma, representing different mineralizing events. For each mineralizing event, lead isotopes may have originated from different sources reflected on the model lead growth curve. Lead iso-

Table 1. Summary of lead isotope ranges for samples showing degrees of compatible isotope signatures.

<b>Intrusions/Formations/Veins</b>	<b><math>^{206}\text{Pb}/^{204}\text{Pb}</math></b>	<b><math>^{207}\text{Pb}/^{204}\text{Pb}</math></b>	<b><math>^{208}\text{Pb}/^{204}\text{Pb}</math></b>
Base metal veins galena	17.50–18.44	15.51–15.61	37.16–38.46
Sulfide veins hosted by Belt Supergroup formations	16.70–17.13	15.57–15.81	36.47–37.11
Elkhorn Mountains Volcanics	18.05–18.18	15.57–15.65	38.27–38.53
Elkhorn Mountains diorite intrusions	17.88–18.35	15.51–15.57	38.29–38.46
Lowland Creek Volcanics	16.86–18.98	15.39–15.70	37.71–38.98
Belt Supergroup formations	10.73–17.18	14.92–15.81	29.83–45.13
Unionville granodiorite	18.01–18.02	15.60–15.64	38.26–38.28
Clancy granodiorite	17.99–18.01	15.56–15.60	38.22–38.23
Aplite/alaskite/pegmatite dikes and sills	17.89–18.17	15.56–15.68	38.22–38.57
Butte granite	17.87–18.10	15.54–15.65	38.11–38.51
Montana Tunnels breccia pipe galena	21.46	15.91	40.38
Golden Sunlight diorite intrusion	17.93	15.48	38.00
Big Belt Mountains intrusions	16.77–18.85	15.31–15.57	37.03–38.92
Big Belt Mountains mineralized rocks	17.66–20.80	15.42–15.73	37.16–39.65
Basin mining district stream bed sediments	17.73–18.16	15.53–15.59	37.37–38.26

*Note.* Data are from this investigation and from previous investigations by Doe and others (1968), Zartman (1992), Dudás and others (2010), Unruh and others (2000), and du Bray and others (2017) and are shown in appendices A–F.

topes from Montana Tunnels plots beyond the lead isotope growth curve representing a future date (fig. 16) caused by an excess of radiogenic lead, most likely generated from *in situ* radioactive decay of uranium and thorium incorporated into the breccia pipe when it formed.

### Satellite Plutons and Intrusions

Lead isotopes plotted on covariant diagrams for the Boulder Batholith satellite plutons and intrusions (figs. 3 and 10) partially overlap the base metal veins, forming a tight cluster of points above and on the 85 Ma mixing line. These plots suggest some of the intrusions originated from a different isotopic source than the base metal veins. Other intrusions that plot on the 85 Ma mixing line and overlap the base metal veins may share the same lead isotope origin. Plutons and intrusions plotted on the model lead growth curves (fig. 17) have model ages varying from 600 Ma to 200 Ma, with most points clustering at 400 Ma. The narrow

model ages suggest the plutons and intrusions originated from the same isotopic source with little variation in lead isotope compositions between intrusive events.

### Lowland Creek Volcanic Field

The LCVF shows a wide range of lead isotope compositions (table 1). On the  $^{206}\text{Pb}/^{204}\text{Pb}$  vs.  $^{207}\text{Pb}/^{204}\text{Pb}$  covariant diagram (fig. 4), LCVF Pb isotopes plot along the 85 Ma mixing line and form three point clusters. On the  $^{206}\text{Pb}/^{204}\text{Pb}$  vs.  $^{208}\text{Pb}/^{204}\text{Pb}$  covariant diagram (fig. 11), LCVF Pb isotopes cluster on the 85 Ma mixing line. Other points are scattered above and on the 66 Ma Big Belt Mountains reference isochron, showing a wide deviation from the mixing line. The two covariant plots (figs. 4 and 11) suggest the LCVF lead isotopes originated from heterogeneous diverse sources of crustal- and mantle-derived magmas. The diversity of lead isotope sources is reflected on the model lead growth curves (fig. 18).

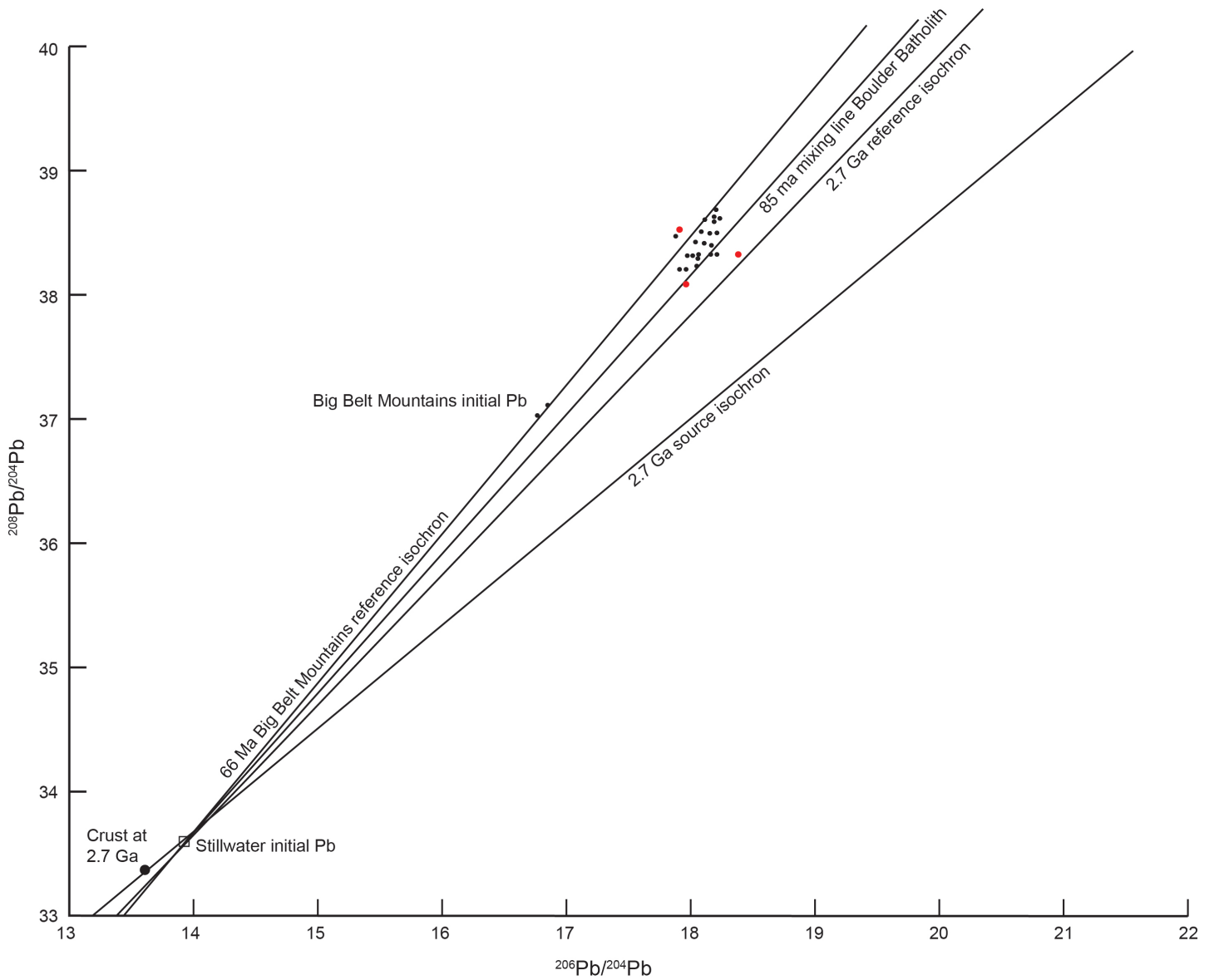


Figure 10. Covariant diagram for  $^{208}\text{Pb}/^{204}\text{Pb}$  vs.  $^{206}\text{Pb}/^{204}\text{Pb}$  plot for Boulder Batholith intrusions published by Doe and others (1968) with additional data generated by this investigation (red points).

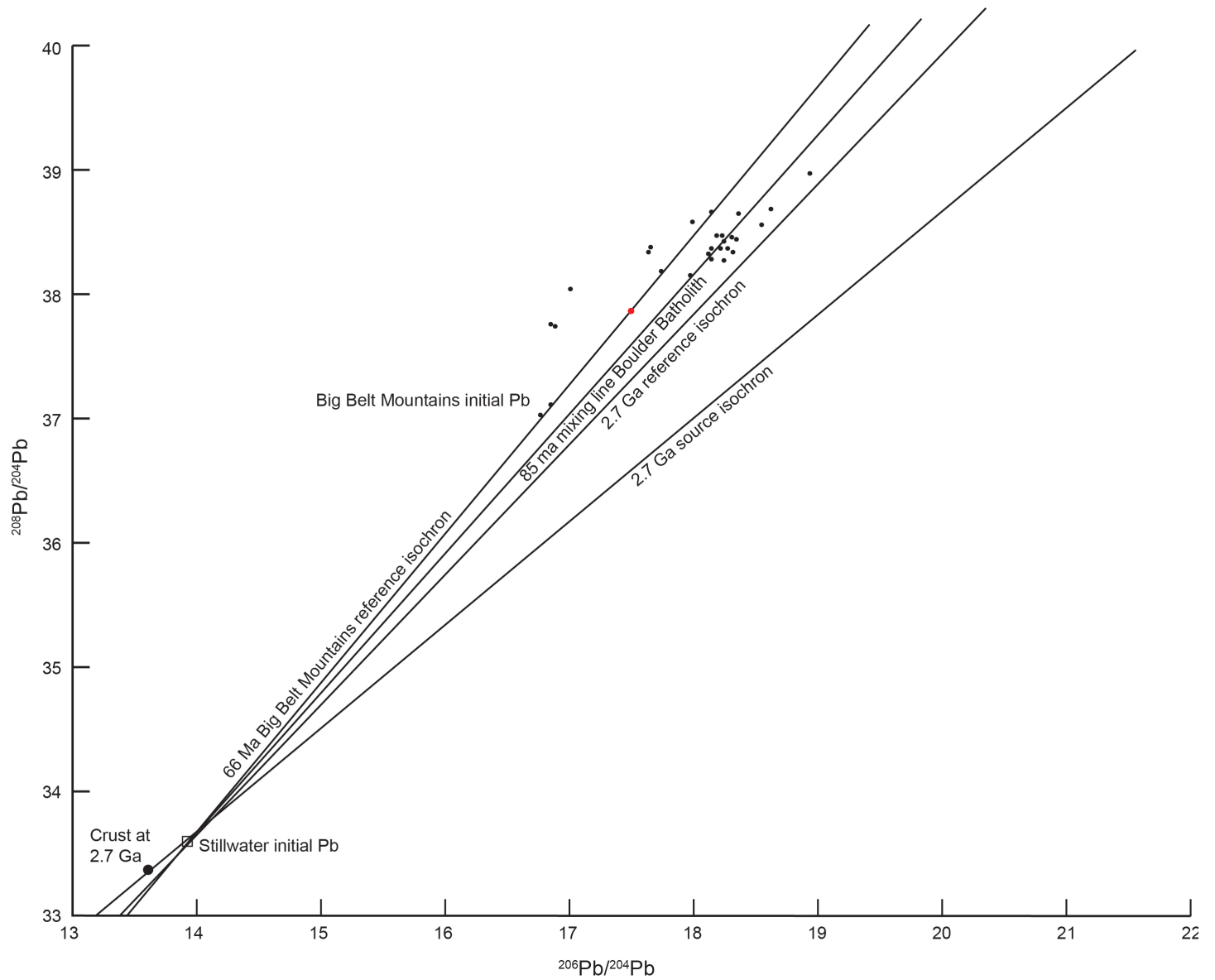


Figure 11. Covariant diagram for  $^{208}\text{Pb}/^{204}\text{Pb}$  vs.  $^{206}\text{Pb}/^{204}\text{Pb}$  plot for Lowland Creek volcanic rocks published by Dudás and others (2010) with additional data generated by this investigation (red point).

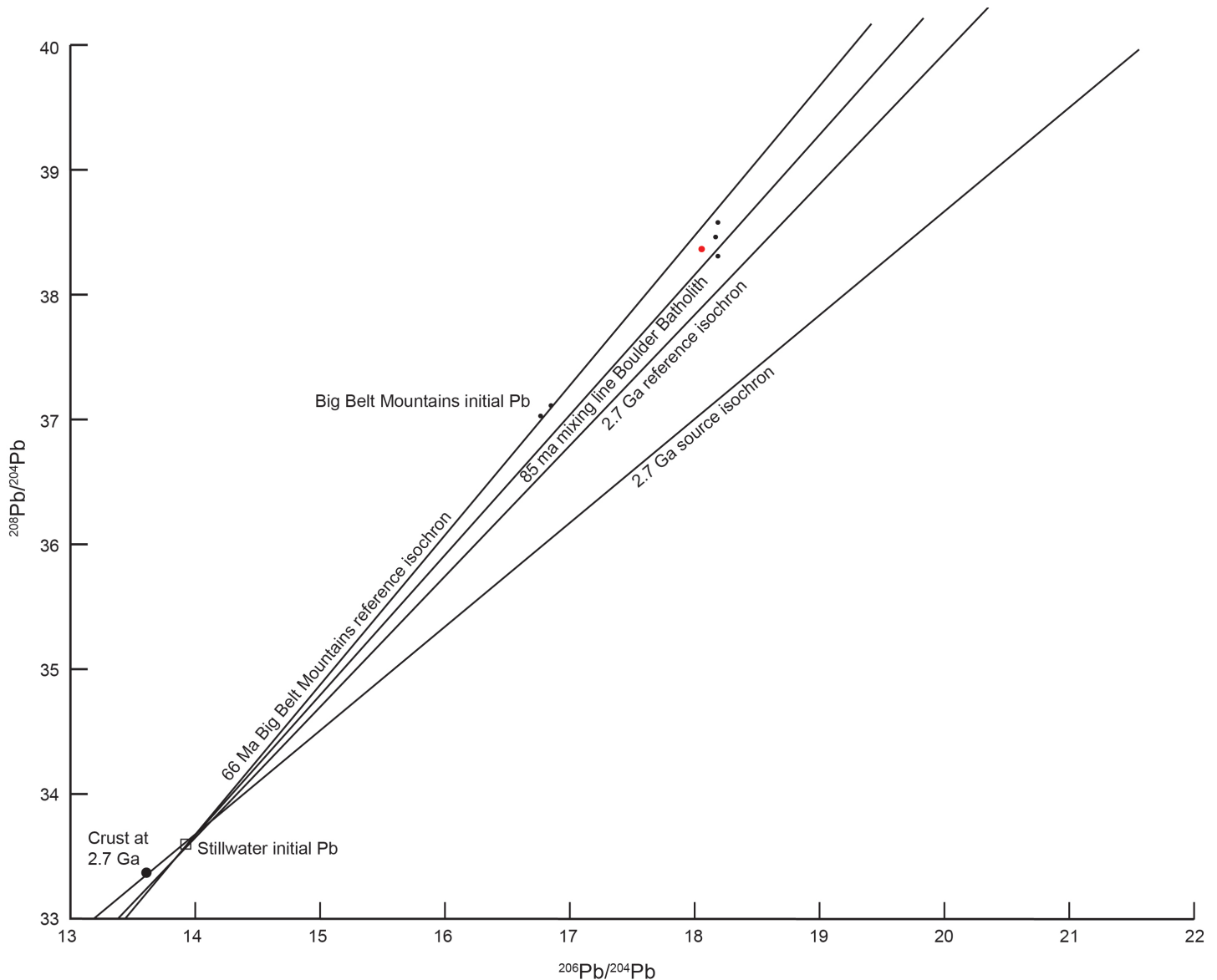


Figure 12. Covariant diagram for  $^{208}\text{Pb}/^{204}\text{Pb}$  vs.  $^{206}\text{Pb}/^{204}\text{Pb}$  plot for Elkhorn Mountains volcanic rocks published by Doe and others (1968) with additional data generated by this investigation (red point).

Model ages vary from 1,200 Ma to 0 Ma and three point clusters similar to the covariant diagrams occur along the model lead growth curves. Based on their lead isotope study, Dudás and others (2010) suggested two magmatic sources for the LCVF eruptions, consisting of a lower to middle crustal source and a lithospheric source.

### Elkhorn Mountains Volcanic Field

Lead isotopes from the EMVF plotted on covariant diagrams fall near the 85 Ma mixing line (figs. 5 and 12) and overlap the satellite pluton point clusters, one of the point clusters for the LCVF, and the base metal veins (figs. 2–4 and 9–11). These diagrams suggest the EMVF isotopes originated from similar sources as the satellite plutons, LCVF, and base metal veins. Model lead growth curves (fig. 19) show lead isotopes

for the EMVF plot with a model age of 400 Ma. This model age is the same for the satellite plutons, LCVF, and base metal veins (figs. 16–18), indicating similar lead isotope sources.

### Stream Sediments

Stream sediment Pb isotopes from the Basin mining district plotted on covariant diagrams are tightly clustered on the 85 Ma mixing line (figs. 6 and 13). The stream sediment plots are similar to the base metal veins, showing the stream sediment Pb isotopes originated from the base metal veins. The stream sediment Pb isotopes represent the Basin mining district veins and the tight clustering of points suggest the Basin mining district veins originated from a single homogenous source during one mineralizing event. Stream sediment lead isotopes plotted on mod-

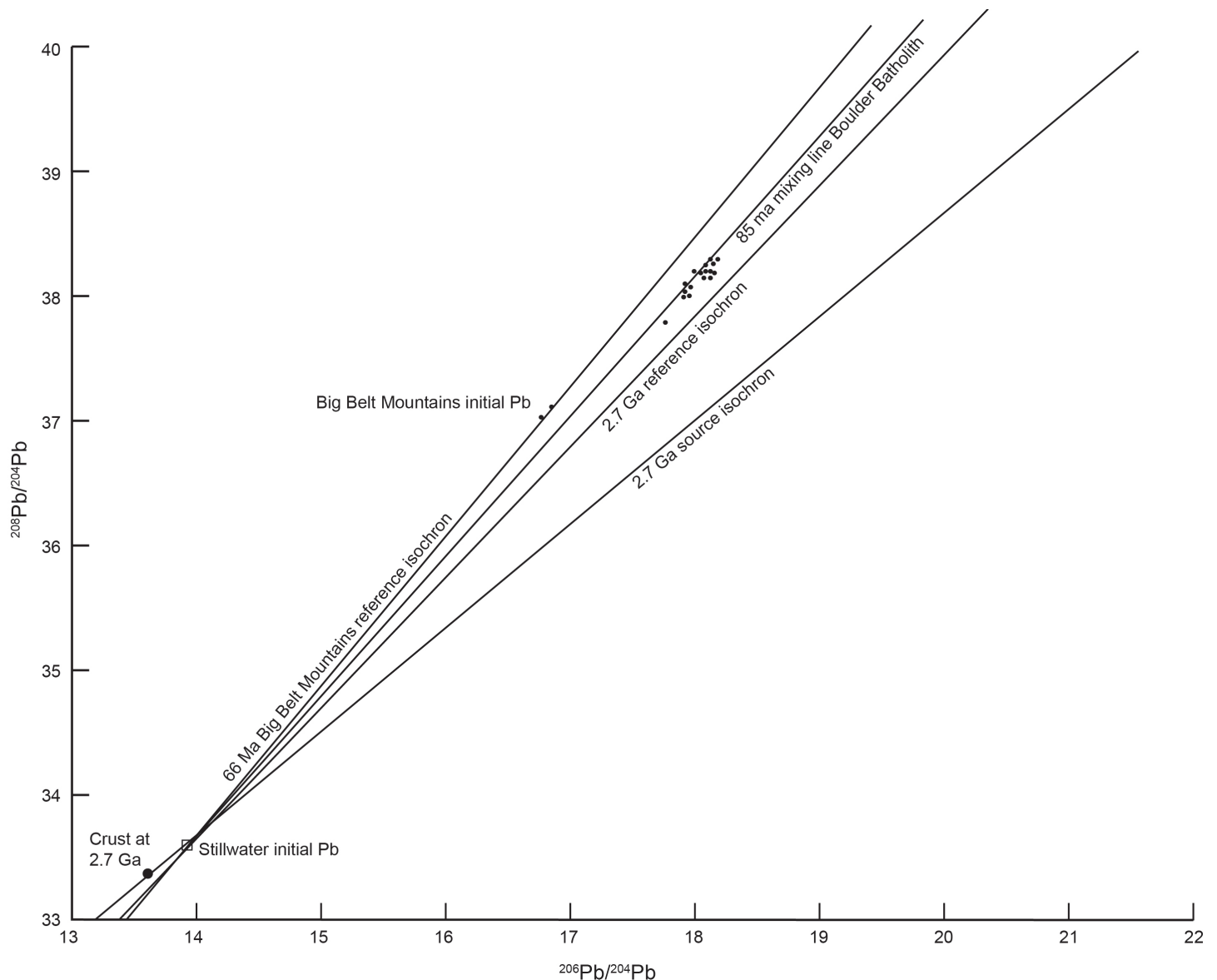


Figure 13. Covariant diagram for  $^{208}\text{Pb}/^{204}\text{Pb}$  vs.  $^{206}\text{Pb}/^{204}\text{Pb}$  plot for stream sediment samples from the Basin mining district (Uhrh and others, 2000).

el lead growth curves (fig. 20) show a clustering of points around a model age of 400 Ma. This model age is shared by the base metal veins, satellite plutons, EMVF, and LCVF (figs. 2–5 and 9–12), demonstrating they have a common isotopic source.

### Big Belt Mountains

The Big Belt Mountains intrusions and mineralized rocks partially overprint the lead isotope compositions from the Boulder Batholith (table 1). On covariant diagrams these primarily plot between the 85 Ma mixing line and the 66 Ma Big Belt Mountains reference isochron (figs. 7 and 14). Lead isotopes plotting below the mixing line in figure 7 indicate they are less radiogenic than the Boulder Batholith isotopes shown in figures 2–6. On the  $^{206}\text{Pb}/^{204}\text{Pb}$  vs.  $^{208}\text{Pb}/^{204}\text{Pb}$  covariant diagram (fig. 14), Pb isotopes plot below the

85 Ma mixing line and below the 2.7 Ga reference isochron. The lead isotope plots in figures 7 and 14 indicate an isotope source contaminated by assimilation of isotopically evolved crustal components including a portion of lithospheric mantle and subcontinental-derived material as suggested by du Bray and others (2017). Lead isotopes for the Boulder Batholith and Big Belt Mountains intrusions are constrained between the 2.7 Ga reference isochron and 66 Ma Big Belt Mountains reference isochron (figs. 2–7 and 9–14), indicating they underwent similar geologic processes during intrusion.

Big Belt Mountains lead isotopes plotted on lead growth curves show a wide range of model lead ages, varying from 1,200 Ma to 0 Ma (fig. 21). This wide variation on model lead ages implies a heterogeneous

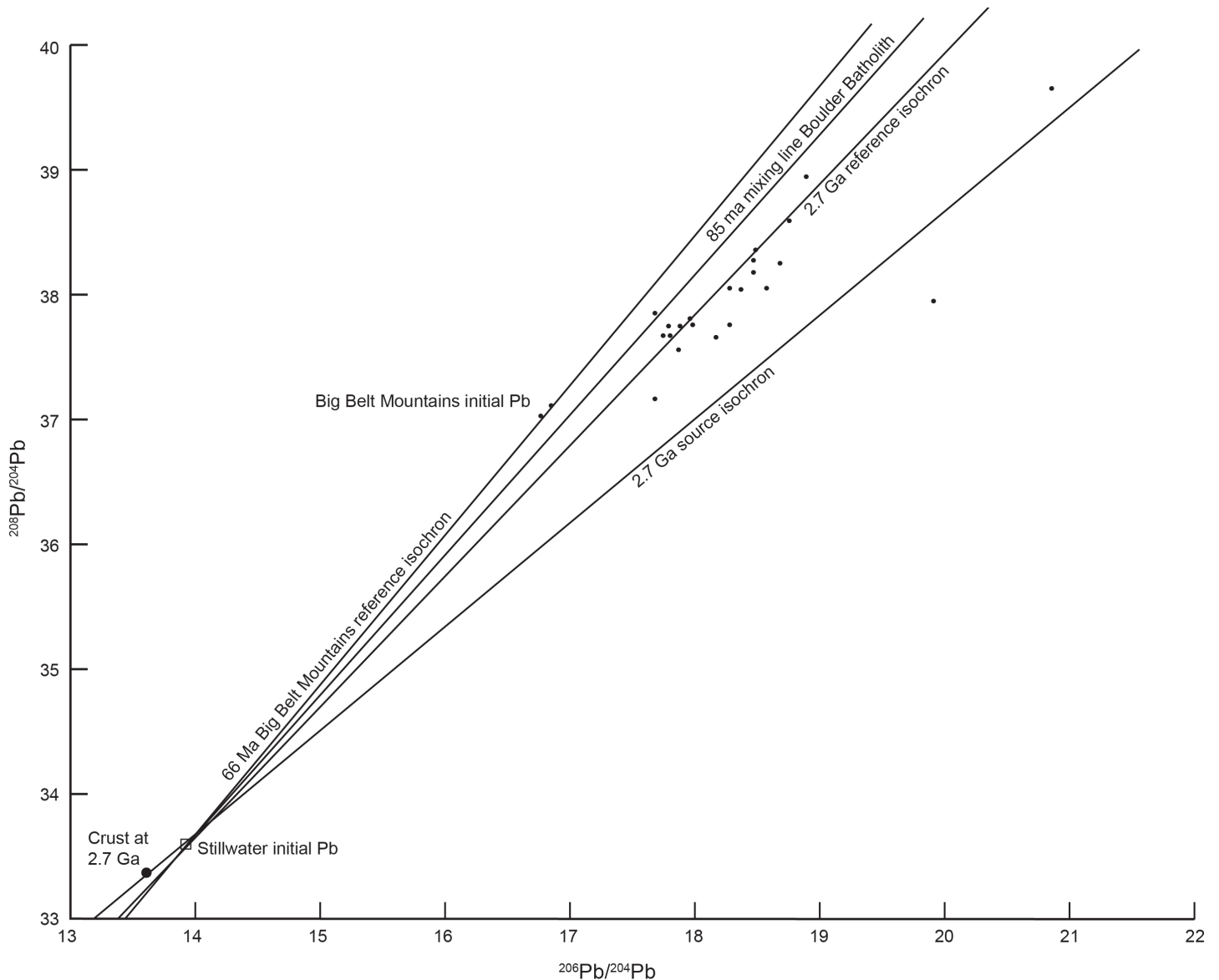


Figure 14. Covariant diagram for  $^{208}\text{Pb}/^{204}\text{Pb}$  vs.  $^{206}\text{Pb}/^{204}\text{Pb}$  plot for the Big Belt Mountains, data published by du Bray and others (2017).

lead isotope source for the Big Belt Mountains Intrusions, as argued for by du Bray and others (2017). The lead growth curves show a clustering of points consistent with model ages of 1,200 Ma, 600 Ma, and from 400 Ma to 0 Ma (fig. 21). Two points plot with future model ages, which could be attributed to *in situ* radioactive decay. Lowland Creek volcanic field lead isotopes show a similar trend, with a clustering of points at model ages of 1,200 Ma, between 800 Ma and 600 Ma, and between 400 Ma and 0 Ma (fig. 18). These similarities in model ages imply both the 68 to 66 Ma Big Belt Mountains intrusions and the 53 to 49 Ma LCVF developed from similar geologic processes and lead isotope sources. Proximity of the Boulder Batholith to the Big Belt Mountains and similar late Cretaceous ages suggest they have similar isotopic sources and petrogenetic histories.

### Belt Supergroup Formations and Sulfide Veins

Most lead isotopes for the Belt Supergroup formations and associated sulfide veins plotted on covariant diagrams are constrained between the 2.7 Ga reference isochron and 2.7 Ga source isochron (figs. 8 and 15), suggesting a crustal isotopic source. The covariant diagrams show the lead isotope source for the Belt Supergroup formations and associated sulfide veins are different from those of the Boulder Batholith and may not be directly related. Belt Supergroup formations and associated sulfide vein lead isotopes plotted on lead growth curves show model ages between 1,200 Ma and 1,000 Ma, which is older than Boulder Batholith model ages (fig. 22). The exception is a cluster of LCVF lead isotope points with a model age of 1,200 Ma (fig. 18). Even though one LCVF

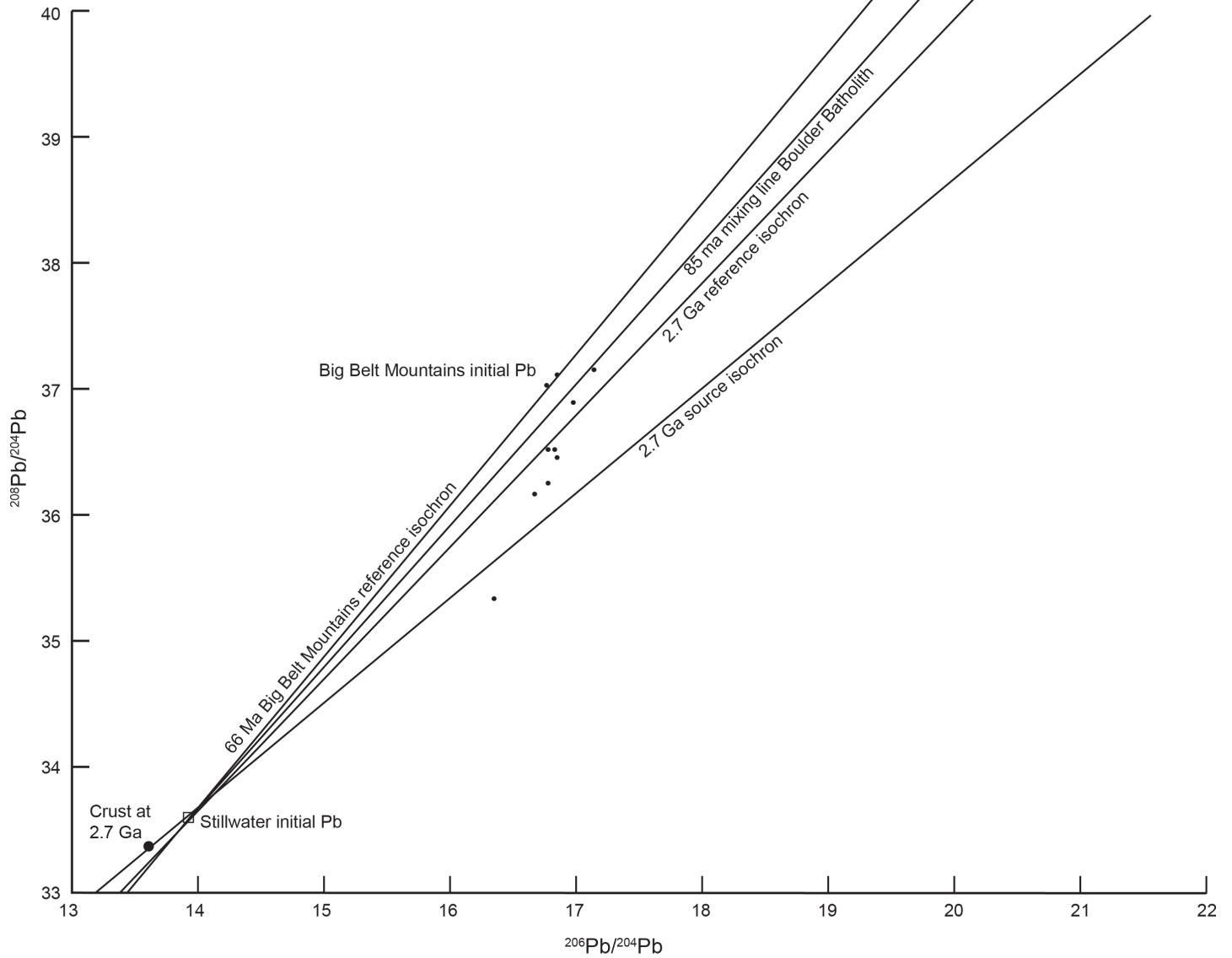


Figure 15. Covariant diagram for  $^{208}\text{Pb}/^{204}\text{Pb}$  vs.  $^{206}\text{Pb}/^{204}\text{Pb}$  plot for the Belt Supergroup formations and hosted sulfide veins, data published by Zartman (1992).

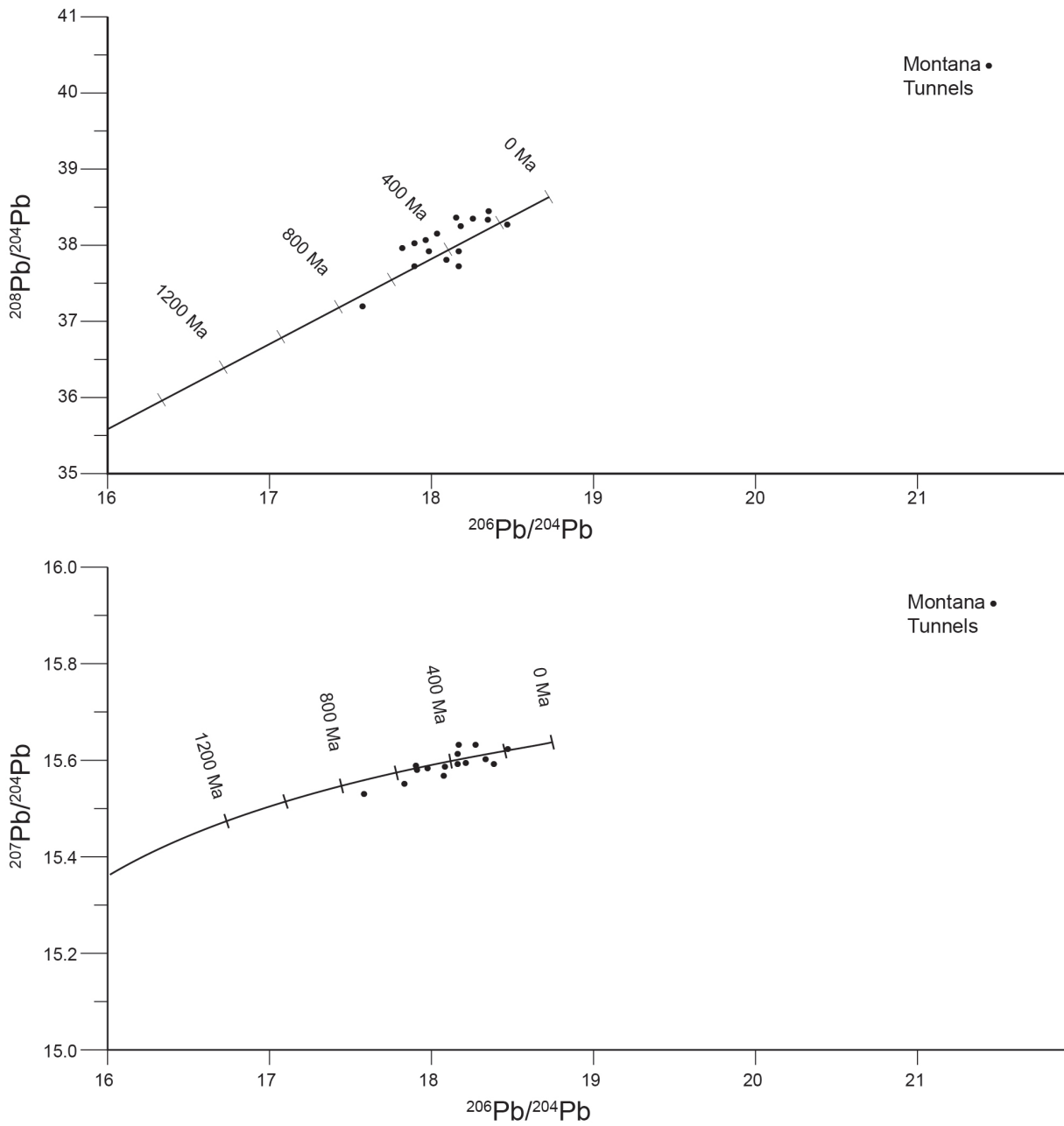


Figure 16. Lead isotope ratios generated by this investigation for galena samples from base metal veins and galena from Montana Tunnels breccia pipe plotted on Stacey and Kramers (1975) model lead isotope growth curves for  $^{206}\text{Pb}/^{204}\text{Pb}$  vs.  $^{207}\text{Pb}/^{204}\text{Pb}$  (below) and  $^{206}\text{Pb}/^{204}\text{Pb}$  vs.  $^{208}\text{Pb}/^{204}\text{Pb}$  ratios.

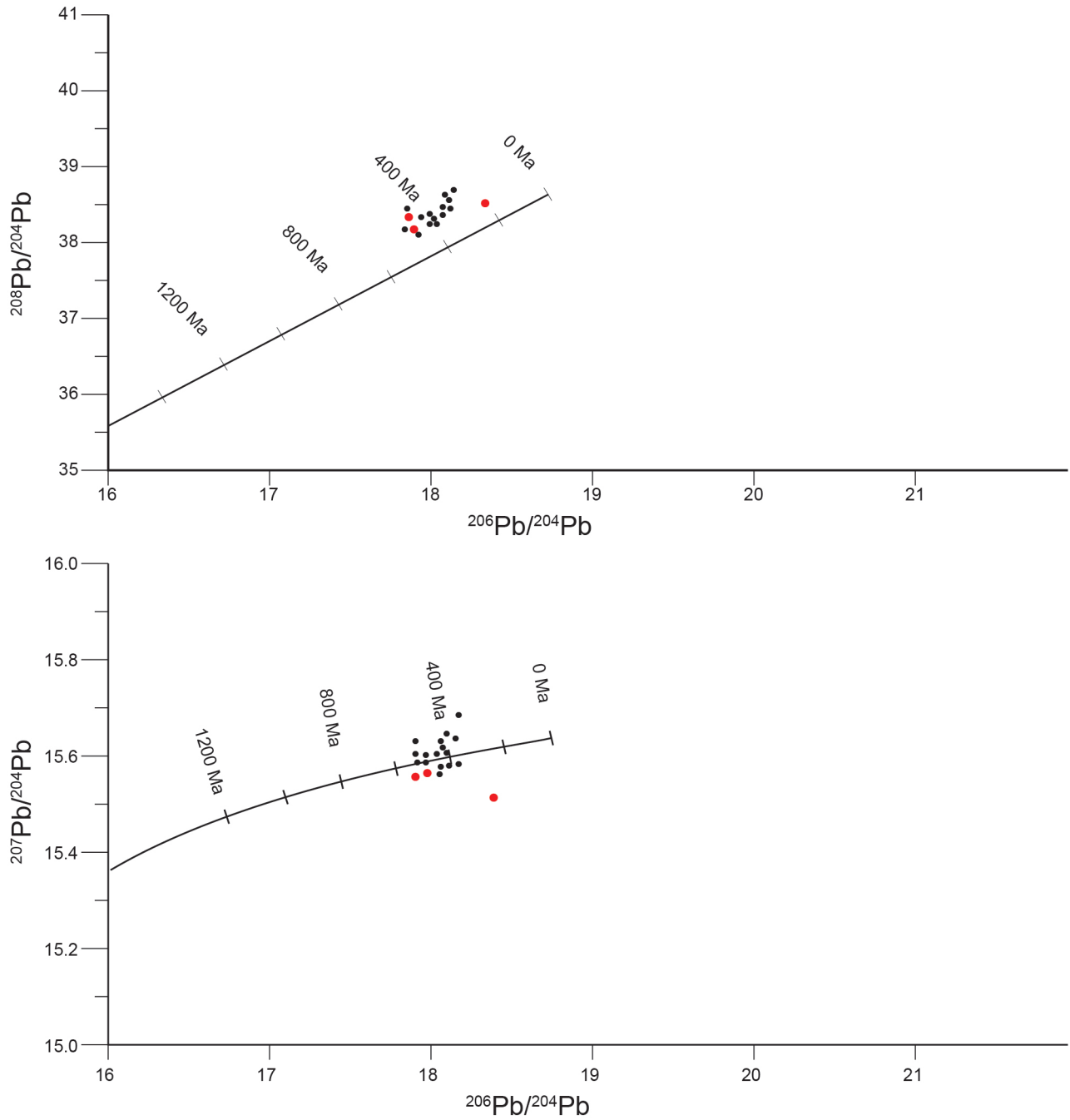


Figure 17. Lead isotope ratios for Boulder Batholith intrusions from data published by Doe and others (1968) with additional data generated by this investigation (red points) plotted on Stacey and Kramers (1975) model lead isotope growth curves for  $^{206}\text{Pb}/^{204}\text{Pb}$  vs.  $^{207}\text{Pb}/^{204}\text{Pb}$  (below) and  $^{206}\text{Pb}/^{204}\text{Pb}$  vs.  $^{208}\text{Pb}/^{204}\text{Pb}$  ratios.

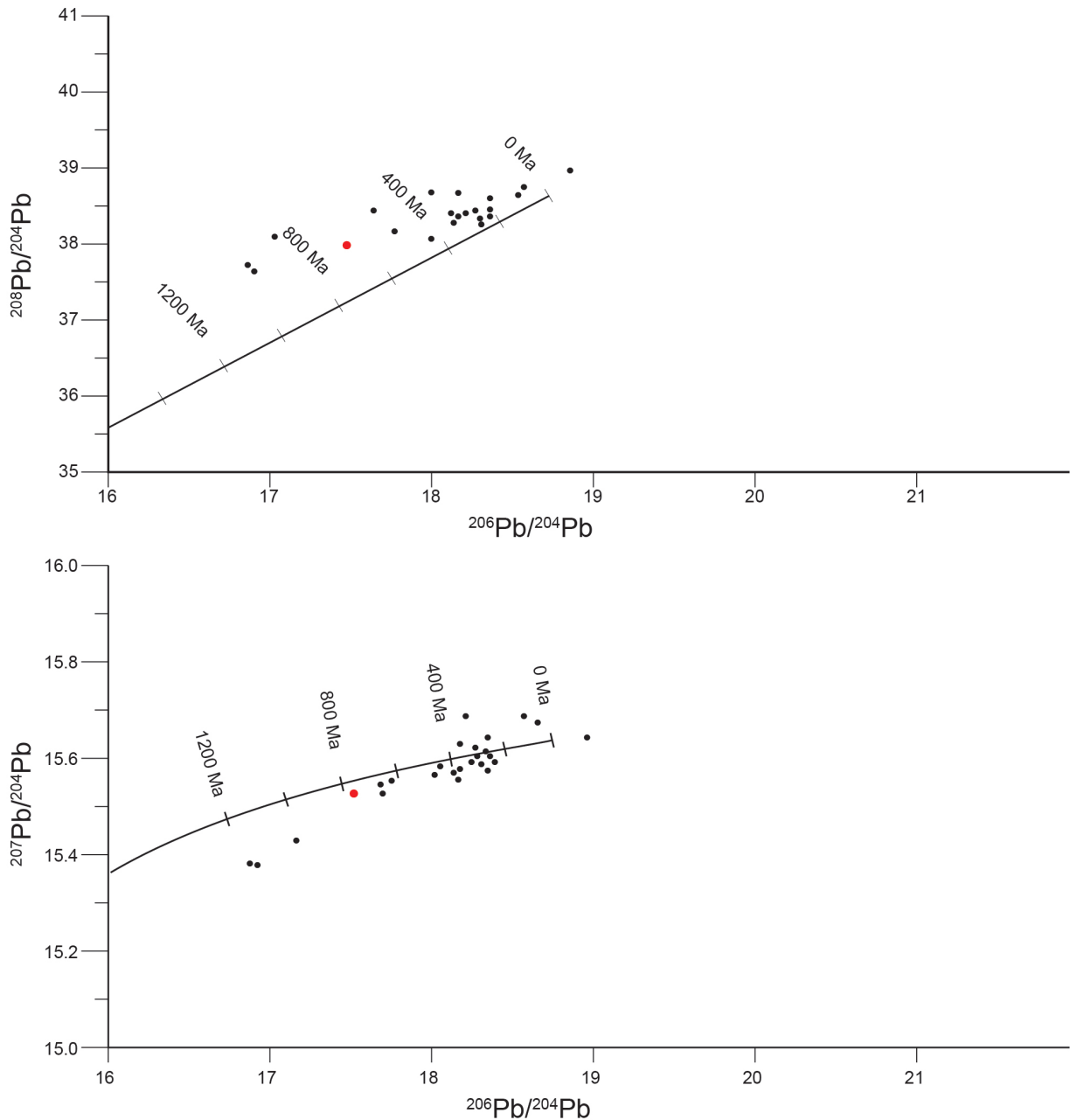


Figure 18. Lead isotope ratios for Lowland Creek volcanic rocks from data published by Dudás and others (2010) with additional data generated by this investigation (red points) plotted on Stacey and Kramers (1975) model lead isotope growth curves for  $^{206}\text{Pb}/^{204}\text{Pb}$  vs.  $^{207}\text{Pb}/^{204}\text{Pb}$  (below) and  $^{206}\text{Pb}/^{204}\text{Pb}$  vs.  $^{208}\text{Pb}/^{204}\text{Pb}$  ratios.

point cluster shares a model age with Belt Supergroup formations, they do not share the same lead isotope source. This is supported by covariant diagrams, in which LCVF lead isotopes plot on the 85 Ma mixing line (fig. 4) and Belt Supergroup formations are constrained between the 2.7 Ga reference isochron and 2.7 Ga source isochron (figs. 8 and 15). When covariant diagrams and lead growth curves of the Boulder Batholith are compared with the Belt Supergroup formations and associated sulfide veins (figs. 2–6, 9–13, and 16–20), it appears the lead isotopes for the Belt Supergroup formations had a different source than the lead isotopes for the Boulder Batholith.

### Magma Source

Based on  $\text{Sr}_i$  values, du Bray and others (2017) report the intrusive rocks of the Big Belt Mountains have a less evolved isotopic source including contributions from the asthenospheric mantle and are less contaminated by crustal rock assimilation than the Boulder Batholith intrusions. Variations of  $^{207}\text{Pb}/^{204}\text{Pb}$  and  $^{208}\text{Pb}/^{204}\text{Pb}$  reflect radiogenic Pb compositions of the magmatic source or the extent of geochemical evolution and the Pb isotopic composition of crustal-derived contaminants. Relative variations of  $^{206}\text{Pb}/^{204}\text{Pb}$  are a function of age of the associated ig-

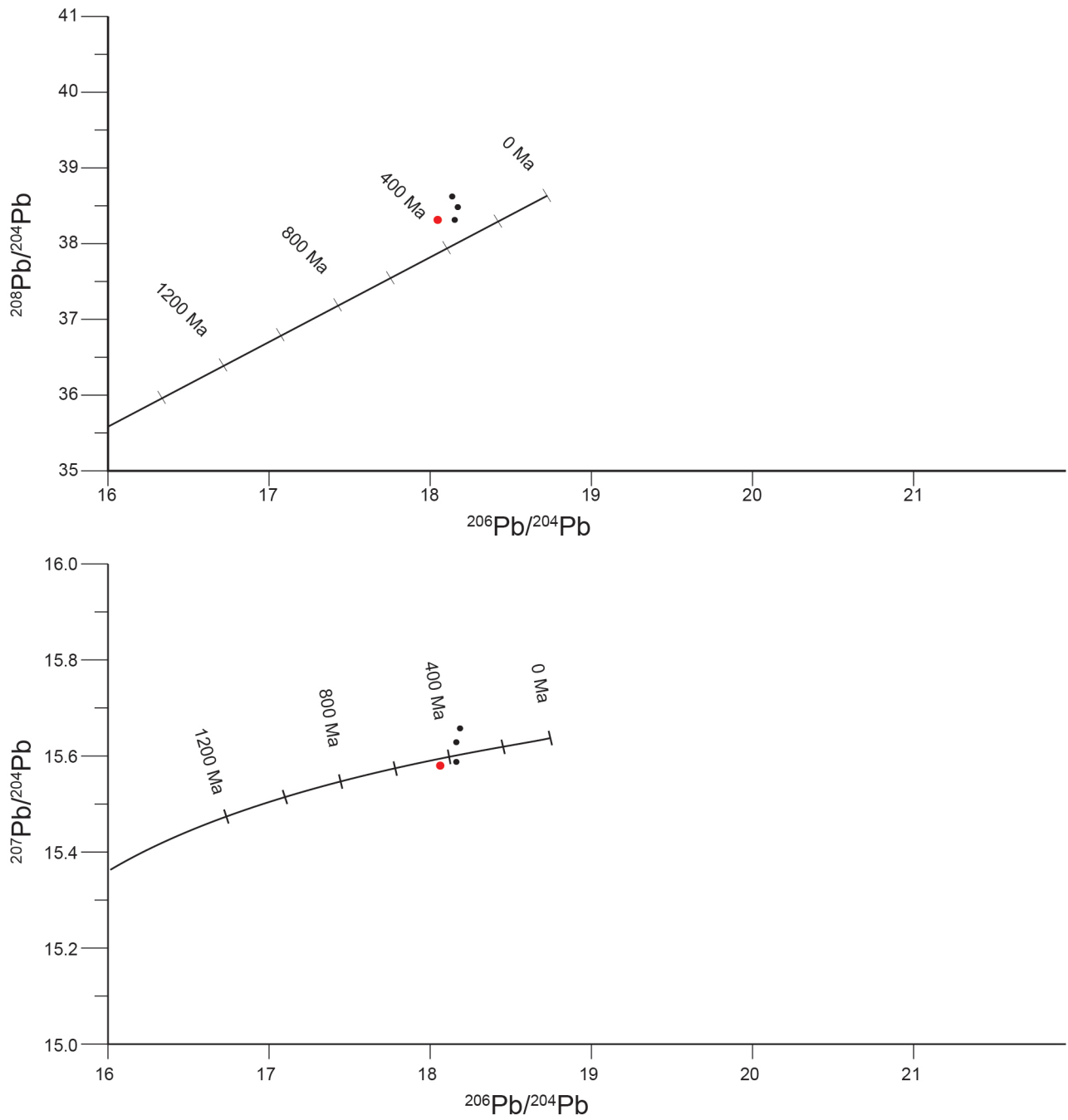


Figure 19. Lead isotope ratios for Elkhorn Mountains volcanic rocks from data published by Doe and others (1968) with additional data generated by this investigation (red points) plotted on Stacey and Kramers (1975) model lead isotope growth curves for  $^{206}\text{Pb}/^{204}\text{Pb}$  vs.  $^{207}\text{Pb}/^{204}\text{Pb}$  (below) and  $^{206}\text{Pb}/^{204}\text{Pb}$  vs.  $^{208}\text{Pb}/^{204}\text{Pb}$  ratios.

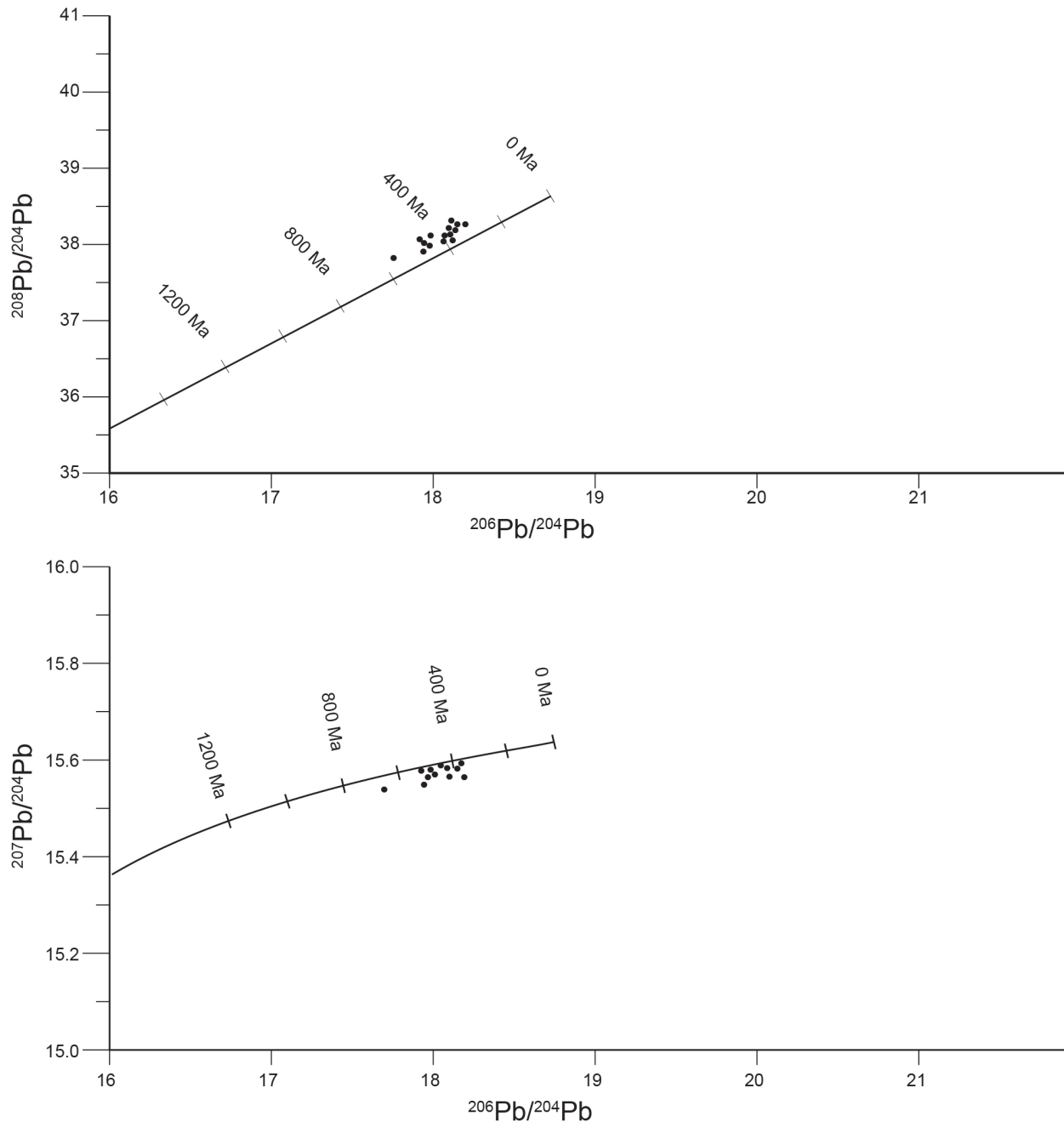


Figure 20. Lead isotope ratios for stream sediments from the Basin mining district from data published by Uhrh and others (2000) plotted on Stacey and Kramers (1975) model lead isotope growth curves for  $^{206}\text{Pb}/^{204}\text{Pb}$  vs.  $^{207}\text{Pb}/^{204}\text{Pb}$  (below) and  $^{208}\text{Pb}/^{204}\text{Pb}$  vs.  $^{206}\text{Pb}/^{204}\text{Pb}$  ratios.

neous rocks and their source. In contrast to the Boulder Batholith intrusions, the Big Belt Mountains intrusions  $^{207}\text{Pb}/^{204}\text{Pb}$  and  $^{208}\text{Pb}/^{204}\text{Pb}$  are less radiogenic, indicating the intrusions are less contaminated by assimilation of isotopically evolved crustal components and include a greater proportion of lithospheric mantle and subcontinental-derived material (du Bray and others, 2017). Boulder Batholith intrusions, on the other hand, have more radiogenic  $^{207}\text{Pb}/^{204}\text{Pb}$  and  $^{208}\text{Pb}/^{204}\text{Pb}$  (table 1) and plot on an 85 Ma mixing line (figs. 2–6, and 9–13) independent of the 66 Ma Big Belt Mountains reference isochron. This indicates

they are more contaminated with assimilated crustal components and have a lesser proportion of subcontinental- and lithospheric mantle-derived material.

The partial melting and mixing of crustal and mantle magmas causes the transfer of U-Th-Pb from the mantle and crust into magmas generated in a subduction zone (Tosdal and others, 1999). Because of U-Th-Pb mixing, lead isotope ratios generated in a subduction-related magma can vary, depending on the degree of mantle, and upper and lower crust melting (Faure, 1977). The volcanic rocks and intrusions of the Boulder Batholith were formed in a volcanic

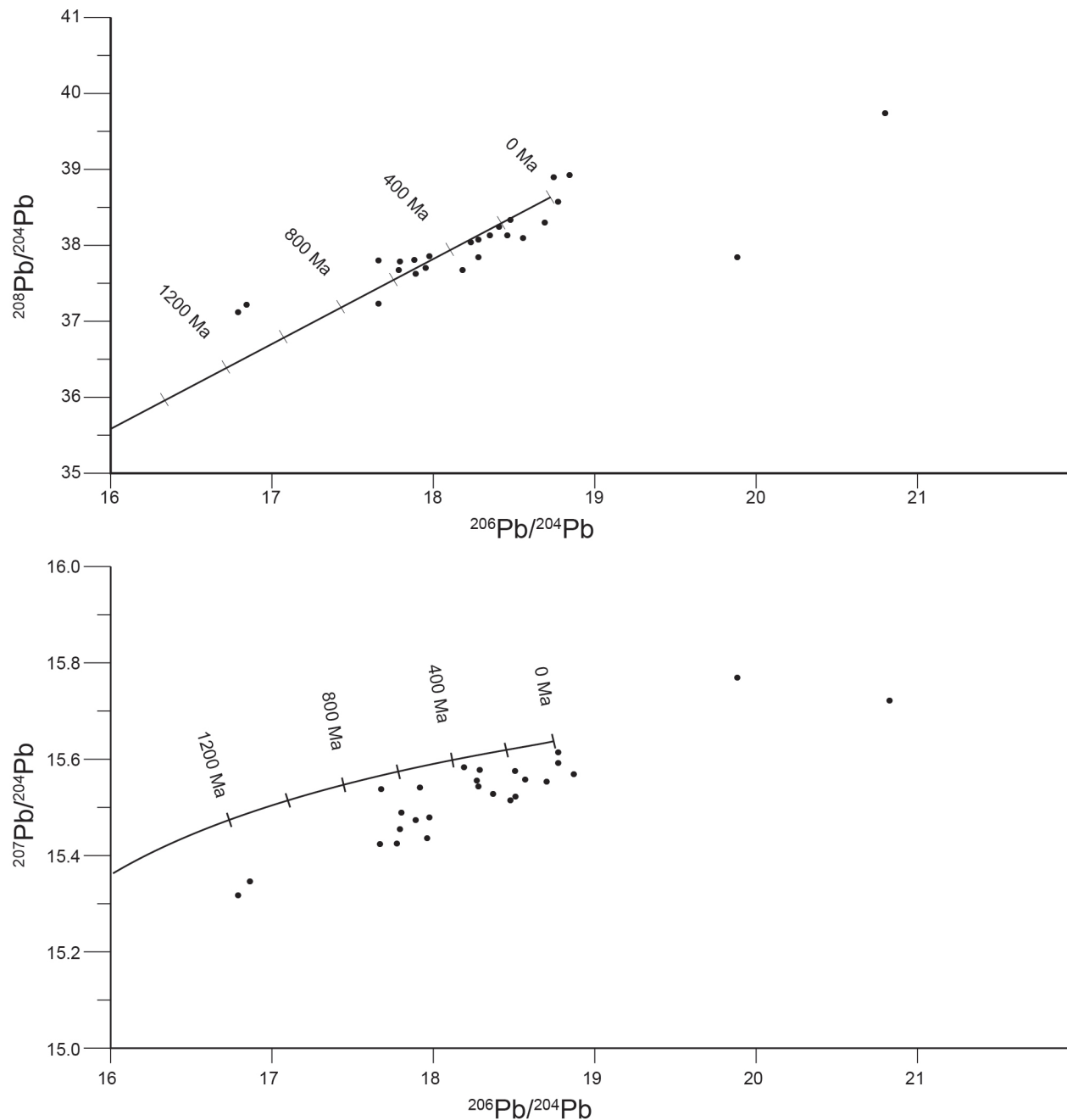


Figure 21. Lead isotope ratios for the Big Belt Mountains from data published by du Bray and others (2017) plotted on Stacey and Kramers (1975) model lead isotope growth curves for  $^{206}\text{Pb}/^{204}\text{Pb}$  vs.  $^{207}\text{Pb}/^{204}\text{Pb}$  (below) and  $^{206}\text{Pb}/^{204}\text{Pb}$  vs.  $^{208}\text{Pb}/^{204}\text{Pb}$  ratios.

back arc environment and originated from subduction-related magmatism (du Bray and others, 2012). The volcanic rocks, intrusions, and base metal vein galena  $^{207}\text{Pb}/^{204}\text{Pb}$  and  $^{208}\text{Pb}/^{204}\text{Pb}$  populations are scattered along 85 Ma mixing lines (figs. 2–6 and 9–13), demonstrating some isotopic diversity in crustal contaminants that assimilated into the magmas by partial melting. Compared to most intrusions in the Boulder Batholith, the diorite intrusion from the Golden Sunlight mine is the least radiogenic intrusion ( $^{207}\text{Pb}/^{204}\text{Pb}$  15.48,  $^{208}\text{Pb}/^{204}\text{Pb}$  38.00) and Lowland Creek volcanic rocks are the most radiogenic ( $^{207}\text{Pb}/^{204}\text{Pb}$  15.70,

$^{208}\text{Pb}/^{204}\text{Pb}$  38.98), showing a balance of magmas or heterogeneous isotopic sources for crustal contaminants that were assimilated into the magmas. In addition, Lowland Creek volcanic rocks show a wide range of  $^{207}\text{Pb}/^{204}\text{Pb}$  ratios (table 1), further suggesting a variable isotopic source for crustal contaminants in magmas that generated these volcanic rocks.

Intrusions in the Big Belt Mountains originated from subduction-related magmatism (du Bray and others, 2017). The proximity of the Big Belt Mountains to the east of the Boulder Batholith and similar ages

imply they originated from the same subduction event. Compared to the Boulder Batholith, the intrusions in the Big Belt Mountains are less radiogenic (du Bray and others, 2017; table 1). Similar to the Boulder Batholith, Pb isotopes for the Big Belt Mountains intrusions have variable ratios, implying source region isotopic heterogeneity and variable contamination from diverse crustal assimilants (du Bray and others, 2017). The less radiogenic flows in the Lowland Creek volcanic rocks could have a higher proportion of derived lithospheric mantle, argued for by Dudás and others (2010), and subcontinental material than the other Boulder Batholith volcanic rocks and intrusions. In addition, the wide range of isotopic diversity in the Lowland Creek volcanic rocks suggests a heterogeneous isotopic composition for crustal contaminants assimilated into the Lowland Creek source magmas.

### Ore Deposit Genesis

The base metal veins in the Boulder Batholith have the characteristics of low to intermediate sulfidation epithermal systems. These systems develop from circulating hydrothermal fluids associated with magmas and could develop several kilometers away from the intrusion site (Cooke and Simmons, 2000). Metals transported by circulating hydrothermal fluids that form epithermal veins are sourced from intrusive bodies, host rocks, and underlying formations (Hayba and others, 1985; Hedenquist and Lowenstern, 1994). Hedenquist and Lowenstern (1994) suggest a cooling magma will discharge vapor and hypersaline-acidic magmatic fluids that can leach metals from host formations; the leached metals and associated isotopes become concentrated in magmatic-derived hydrothermal fluids. The metal-enriched, magmatic-derived hydrothermal fluids are transported, mixed with heated circulating meteoric fluids, and vented through fractures developing epithermal veins.

Galena from two types of ore deposits, base metal veins, and a breccia pipe were sampled for lead isotope analysis. Lead isotope compositions for the galena samples overlap isotope populations from the intrusive and volcanic rocks (table 1), demonstrating the intrusions and volcanic rocks hosting the base metal veins are in isotopic equilibrium. This relationship implies base metal vein lead has the same isotopic source as the igneous rocks and could have been derived from magmatic fluids exsolved from igneous intrusions. Based on Pb isotopic compositions between galena from veins and feldspar from plutons, Doe and others (1968) concluded a genetic relationship between the plutons and base metal veins, suggesting the ore fluids could have originated from

igneous rocks reflecting the magmatic lead isotope source.

Lead isotopes for the Boulder Batholith veins overlap the intrusions and volcanic rocks, implying the metals that developed the veins were sourced from intrusion-generated magmatic fluids. There is Pb, Sr, and Nd isotopic evidence the magmas that developed the Boulder Batholith and Big Belt Mountains intrusions and volcanic rocks assimilated crustal rocks (du Bray and others, 2017). Physical evidence for the assimilation of Proterozoic crustal rocks into the magmas when they were generated includes inherited zircons with core Proterozoic ages and rim Cretaceous ages for the Boulder Batholith intrusions (Lund and others, 2002). Intrusions in the Butte, Emery, and Oro Fino districts also include Proterozoic age inherited zircons (Field and others, 2005; Korzeb and others, 2018; Korzeb and Scarberry, in press).

Cooling intrusions exsolving metal-enriched hypersaline fluids that become diluted with circulating meteoric waters or low to moderate density magmatic-derived fluids will rise to shallow depths, leading to the development of epithermal veins (Rottier and others, 2018). There is indirect evidence that metals and sulfur that formed the Boulder Batholith epithermal veins could have been derived from intrusions that assimilated Proterozoic crustal rocks. Field and others (2005), using sulfur isotope data, argued that the sulfur found in the Butte district veins was sourced from magmas contaminated with evaporates from assimilated middle Proterozoic Belt Supergroup rocks. The cooling magma contaminated with assimilated Proterozoic crustal rocks exsolved metal- and sulfur-enriched magmatic fluids, leading to the development of epithermal veins. In addition to the Butte mining district, veins in the Emery and Oro Fino mining districts have sulfur isotope compositions that suggest they developed from a magmatic source that assimilated Proterozoic crustal rocks (Korzeb and others, 2018; Zimmerman, 2016; Korzeb and Scarberry, in press).

Proterozoic crustal rocks assimilated into magmas during intrusion may have enriched the magmas in metals and sulfur. During the Proterozoic, Belt Supergroup sediments became locally metal-enriched from hydrothermal fluids venting on the sea floor and concentrating in the ocean sediments (Box and others, 2012). Lead isotope compositions indicate the magmas that generated the Boulder Batholith intrusions assimilated Archean to Proterozoic crust. Lead isotope compositions further demonstrate the epithermal veins are directly related to intrusions,

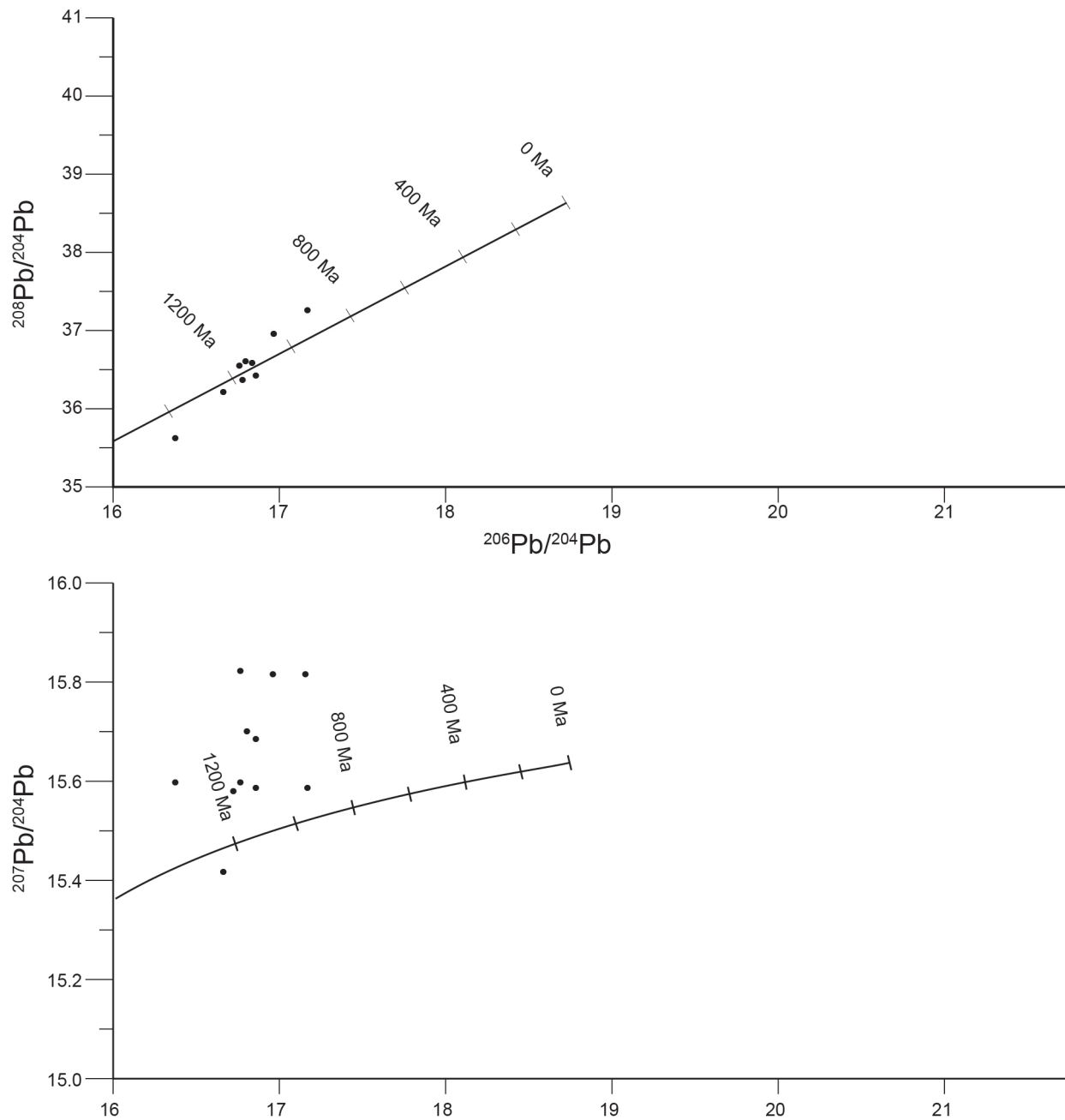


Figure 22. Lead isotope ratios for Belt Supergroup formations and hosted sulfide veins from data published by Zartman (1992) plotted on Stacey and Kramers (1975) model lead isotope growth curves for  $^{206}\text{Pb}/^{204}\text{Pb}$  vs.  $^{207}\text{Pb}/^{204}\text{Pb}$  (below) and  $^{206}\text{Pb}/^{204}\text{Pb}$  vs.  $^{208}\text{Pb}/^{204}\text{Pb}$  ratios.

and hydrothermal fluids were sourced from magmatic fluids exsolving from cooling intrusions. Proterozoic crustal rocks assimilated into Boulder Batholith magmas contributed Proterozoic age inherited zircons, sulfur isotopes with Belt Supergroup signatures, and, in some cases, metal enrichment. Intrusions related to epithermal vein development probably assimilated metal-enriched Belt Supergroup rocks that contributed metals and sulfur to the melt. When these intrusions cooled, they exsolved metal-enriched hypersaline fluids (Rottier and others, 2018) that led to the development of the Boulder Batholith epithermal veins.

Ages for base metal veins representing one of the mineralizing events in the Boulder Batholith took place from 75.12 Ma to 73.1 Ma (Olson and others, 2017). These ages overlap an aplite intrusion age of 74.5 Ma (Korzeb and Scarberry, in press). The overlapping ages suggest a geochronological link between the aplite intrusive event and epithermal vein development. Lead isotope ratios from base metal vein galena and aplite intrusions (table 1; figs. 2, 3, 9, and 10) overlap, indicating isotopic equilibrium between the base metal veins and aplite. The overlapping of lead isotopes and ages between the base metal veins and aplite intru-

sions suggest the hydrothermal fluids that developed the veins were magmatic fluids sourced from the same magma that intruded the aplite dikes and sills.

Galena from the Montana Tunnels breccia pipe has elevated radiogenic lead compared to the base metal veins galena (table 1). The elevated radiogenic lead suggest the breccia pipe developed from a different lead isotope source compared to the base metal veins and could be a reflection of the process that formed the breccia pipe. The breccia pipe is reported to have the characteristics of a maar volcano (Sillitoe and others, 1985) and originated during the eruption of the Lowland Creek volcanic field. Sillitoe and others (1985) concluded the breccia pipe developed from phreatomagmatic explosive activity caused by the interaction of ground water with an ascending quartz latite magma. As the magma was being intruded and the maar volcano was erupting, magmatic fluids mixed with an influx of meteoric water. The underlying Butte granite could be a source for U and Th that was leached from the granite by meteoric waters (Dodd, 1981). The influx of meteoric water into the breccia pipe during mineralization may have introduced uranium and thorium into the primary magmatic fluids. *In situ* radioactive decay of the added U and Th may have generated an enrichment of radiogenic Pb isotopes that occur in the Montana Tunnels galena sample.

## CONCLUSION

Lead isotope compositions for base metal veins, breccia pipe, plutons, and volcanic rocks indicate they originated from a common source. The magmas that generated the Boulder Batholith intrusions were derived from partial melting of lithospheric mantle- and subcontinental-derived material in a subduction zone similar to the nearby Belt Mountains, as suggested by du Bray and others (2017). Mixing of Pb isotopes imply the magmas generated from partial melting of mantle and subcontinental crust assimilated Proterozoic crust into the melts. Variations in Pb isotope ranges between plutons and volcanic rocks indicate heterogeneous or variable isotopic sources. The assimilation of Proterozoic crust into the magmas contributed inherited zircons to the melts. The inherited zircons have Proterozoic cores with Cretaceous age rims, and sulfide minerals have sulfur isotopes with Belt Supergroup compositions (Lund and others, 2002; Field and others, 2005; Korzeb and others, 2018; Korzeb and Scarberry, in press), implying Proterozoic rocks were assimilated into the generating magmas.

Lead isotopes for base metal vein galena samples overlap the intrusions and volcanic rocks hosting the veins, suggesting isotopic equilibrium between the veins, volcanic rocks, and intrusions. The intrusions, veins, and volcanic rocks could have had similar isotopic sources. This overlapping of Pb isotopes implies the hydrothermal fluids that generated the veins was sourced from cooling magmas that assimilated Belt Supergroup rocks. The intrusions that contributed magmatic fluids to vein development may have been enriched in metals by assimilating Belt Supergroup formations. Belt Supergroup formations are known to be locally enriched in sulfides that originated from hydrothermal activity during the Proterozoic (Box and others, 2012). Assimilation of these formations into a magma might enhance the metal content of the melt and contribute sulfur isotopes with a Belt Supergroup signature. Sulfur isotopes reflecting a Belt Supergroup origin are known to occur in epithermal base metal veins from the Butte, Emery, and Oro Fino mining districts (Field and others, 2005; Zimmerman, 2016; Korzeb and others, 2018; Korzeb and Scarberry, in press).

Galena from the Montana Tunnels breccia pipe has more radiogenic Pb than galena from the base metal veins. The increase in radiogenic Pb compared to the base metal veins, volcanic rocks, and plutons indicates a different isotopic lead source or might be caused by the geologic process that formed the breccia pipe. The breccia pipe developed from phreatomagmatic explosive activity caused by the interaction of groundwater with an ascending quartz latite magma (Sillitoe and others, 1985). Groundwater enriched in uranium and thorium could be leached from the underlying Butte granite (Dodd, 1981) and mixed with magmatic fluid exsolving from the quartz latite magma adding U and Th to the breccia pipe. *In situ* radioactive decay of U and Th introduced into the breccia pipe from meteoric water may have increased the radiogenic lead concentration of the breccia pipe galena.

## ACKNOWLEDGMENTS

This research was funded by Montana Technological University of the University of Montana seed grant program. I wish to thank Kaleb Scarberry, Montana Bureau of Mines and Geology, who provided samples for this research and valuable suggestions as this study was progressing. I also would like to thank Susan Smith, who drafted the figures used in this publication, Susan Barth, who did the final edits, and Phyllis Hargrave, Montana Bureau of Mines and Geology, who reviewed the manuscript. I extend a

special thank you to Francis Dudás, Massachusetts Institute of Technology, and John Ridley, Department of Geosciences, Colorado State University, Fort Collins, Colorado for their review. Their comments and suggestions greatly improved the final manuscript and data interpretation.

## REFERENCES

- Amelin, Y., Davis, D.W., and Davis, W.J., 2005, Decoupled fractionation of even-and odd-mass isotopes of Pb in TIMS: Goldschmidt Conference Abstracts 2005, Non-Traditional Stable Isotopes, p. A215.
- Berger, B.R., Hildenbrand, T.G., and O'Neill, J.M., 2011, Control of Precambrian basement deformation zones on emplacement of the Laramide Boulder Batholith and Butte mining district, Montana, United States: U.S. Geological Survey Scientific Investigations Report 2011–5016, 29 p.
- Box, S.E., Bookstrom, A.A., and Anderson, R.G., 2012, Origins of mineral deposits, Belt-Purcell Basin, United States and Canada: An introduction: *Economic Geology*, v. 107, p. 1081–1088.
- Cooke, D.R., and Simmons, S.F., 2000, Characteristics and genesis of epithermal gold deposits, in Hagemann, S.G., and Brown, P.E., eds.: *Gold in 2000, Reviews in economic geology*, Society of Economic Geologists, v. 13, p. 221–244.
- Dodd, S. P., 1981, The mineralogy, petrology and geochemistry of the uranium-bearing vein deposits near Boulder, Montana, and their relationship to faulting and hot spring activity: Western Washington University, M.S. thesis, 71 p.
- Doe, B.R., Tilling, R.I., Hedge, C.E., and Klepper, M.R., 1968, Lead and strontium isotope studies of the Boulder Batholith, southwestern Montana: *Economic Geology*, v. 63 p. 884–906.
- Doe, B.R., and Zartman, R.E., 1979, Plumbotectonics I, The Phanerozoic, in Barnes, H.L., ed., *Geochemistry of hydrothermal ore deposits*, 2nd ed.: New York, Wiley Interscience, p. 22–70.
- du Bray, E.A., Aleinikoff, N.J., and Lund, K., 2012, Synthesis of petrographic, geochemical, and isotopic data for the Boulder Batholith, southwest Montana: U.S. Geological Survey Professional Paper 1793, 39 p.
- du Bray, E.A., Unruh, D.M., and Hofstra, A.H., 2017, Isotopic data for Late Cretaceous intrusions and associated altered and mineralized rocks in the Big Belt Mountains, Montana: U.S. Geological Survey Data Series 1040, 12 p.
- Dudás, F.Ö., Ispolatov, V.O., Harlan, S.S., and Snee, L.W., 2010, 40Ar/39Ar geochronology and geochemical reconnaissance of the Eocene Lowland Creek volcanic field, west-central Montana: *Journal of Geology*, v. 118, p. 295–304.
- Faure, Gunter, 1977, *Principles of isotope geochemistry*, 2nd edition: New York, John Wiley and Sons, 464 p.
- Field, C.W., Zhang, L., Dilles, J.H., Rye, R.O., and Reed, M.H., 2005, Sulfur and oxygen isotopic record in sulfate and sulfide minerals of early, deep, pre-main stage porphyry Cu-Mo and late main stage base-metal mineral deposits, Butte district, Montana: *Chemical Geology*, v. 215, p. 61–93.
- Grunig, J.K., Guilbert, J.M., and Zeihen, L.G., 1961, Discussions, lead isotopes in ores and rocks of Butte, Montana: *Economic Geology*, v. 56, p. 215–216.
- Hayba, D.O., Bethke, P.M., Heald, P., and Foley, N.K., 1985, Geologic, mineralogic, and geochemical characteristics of volcanic-hosted epithermal precious-metal deposits, in Berger, B.R., and Bethke, P.M., eds., *Geology and geochemistry of epithermal systems: Reviews in Economic Geology*, v. 2, Society of Economic Geologists, p. 129–167.
- Hedenquist, J.W., and Lowenstern, J.B., 1994, The role of magmas in the formation of hydrothermal ore deposits: *Nature*, v. 370, p. 519–527.
- Kalakay, T.J., John, B.E., and Lageson, D.R., 2001, Fault-controlled pluton emplacement in the Sevier fold-and-thrust belt of southwest Montana, USA: *Journal of Structural Geology*, v. 23, p. 1151–1165.
- Korzeb, S.L., Scarberry, K.C., and Zimmerman, J.L., 2018, Interpretations and genesis of Cretaceous age veins and exploration potential for the Emery mining district, Powell County, Montana: *Montana Bureau of Mines and Geology Bulletin* 137, 49 p.
- Korzeb, S.L., and Scarberry, K.C., in press, Genesis and exploration potential for Eocene age veins of the Oro Fino mining district, Deer Lodge County, Montana: *Montana Bureau of Mines and Geology Bulletin*.
- Lageson, D.R., Schmitt, J.G., Horton, B.K., Kalakay, T.J., and Burton, B.R., 2001, Influence of Late Cretaceous magmatism on the Sevier orogenic wedge, western Montana: *Geology*, v. 29, p. 723–726.

- Lawson, R.W., Tarrant, B.R., and Gallagher, A.L., 1937, *Geology of the Tuxedo mining district: Butte, Montana School of Mines B.S. thesis*, 35 p.
- Lonn, J., and Elliott, C., 2010, A walking tour of the Eocene Anaconda detachment fault on Stucky Ridge near Anaconda, Montana: *Northwest Geology*, v. 39, p. 81–90.
- Lund, K., Aleinikoff, J.N., Kunk, M.J., and Unruh, D.M., 2007, SHRIMP U-Pb and  $^{40}\text{Ar}/^{39}\text{Ar}$  age constraints for relating plutonism and mineralization in the Boulder Batholith region, Montana, in Lund, K., ed., *Earth science studies in support of public policy development and land stewardship; Headwaters Province, Idaho and Montana: U.S. Geological Survey Circular C 1350*, p. 39–42.
- Lund, K., Aleinikoff, J.N., Kunk, M.J., Unruh, D.M., Zeihen, G.D., Hodges, W.C., du Bray, E.A., and O'Neill, J.M., 2002, SHRIMP U-Pb and  $^{40}\text{Ar}/^{39}\text{Ar}$  age constraints for relating plutonism and mineralization in the Boulder Batholith region, Montana: *Economic Geology*, v. 97, p. 241–267.
- Mahoney, J.B., Pignotta, G.S., Ihinger, P.D., Wittkop, C., Balgord, E.A., Potter, J.J., and Leistikow, A., 2015, *Geologic relationships in the northern Helena Salient, Montana: Geology of the Elliston Region: Northwest Geology*, v. 44, p. 109–135.
- Martin, M., Dilles, J., and Proffett, J.M., 1999, U-Pb geochronologic constraints for the Butte porphyry system: *Geological Society of America Abstracts with Programs*, v. 31, no. 7, p. A380.
- McCallum, I.S., Thurber, M.W., O'Brien, H.E., and Nelson, B.K., 1999, Lead isotopes in sulfides from the Stillwater complex, Montana: Evidence for subsolidus remobilization: *Contributions in Mineralogy and Petrology*, v. 137, p. 206–219.
- Murthy, V.R., and Patterson, C., 1961, Lead isotopes in ores and rocks of Butte, Montana: *Economic Geology* v. 56, p. 59–67.
- Olson, N.H., Dilles, J.H., Kallio, I.M., Horton, T.R., and Scarberry, K.C., 2016, *Geologic map of the Ratio Mountain 7.5 quadrangle, southwest Montana: Montana Bureau of Mines and Geology ED-MAP-10, scale 1:24,000*.
- Olson, N.H., Sepp, M.D., Dilles, J.H., Mankins, N.E., Blessing, J.M., and Scarberry, K.C., 2017, *Geologic map of the Mount Thompson 7.5 quadrangle, southwest, Montana: Montana Bureau of Mines and Geology EDMAP-11, scale 1:24,000*.
- Portner, R.A., Hendrix, M.S., Stalker, J.C., Miggins, D.P., and Sheriff, S.D., 2011, Sedimentary response to orogenic exhumation in the northern Rocky Mountain Basin and Range province, Flint Creek basin, west-central Montana: *Canadian Journal of Earth Sciences*, v. 48, p. 1131–1153.
- Robinson, G.D., Klepper, M.R., and Obradovich, J.D., 1968, Overlapping plutonism, volcanism, and tectonism in the Boulder Batholith region, western Montana: *Geological Society of America Memoir* 116, p. 557–576.
- Rottier, B., Kouzmanov, K., Casanova, V., Wälle M., and Fontboté, L., 2018, Cyclic dilution of magmatic metal-rich hypersaline fluids by magmatic low-salinity fluid: A major process generating the giant epithermal polymetallic deposit of Cerro de Pasco, Peru: *Economic Geology*, v. 113, p. 825–856.
- Rutland, C., Smedes, H., Tilling, R., and Greenwood, W., 1989, Volcanism and plutonism at shallow crustal levels: The Elkhorn Mountains Volcanics and the Boulder Batholith, southwestern Montana, in Henshaw, P., ed., *Volcanism and plutonism of western North America; v. 2, Cordilleran volcanism, plutonism, and magma generation at various crustal levels, Montana and Idaho, Field trips for the 28th International Geological Congress: American Geophysical Union, Monograph*, p. 16–31.
- Scarberry, K.C., Korzeb, S.L., and Smith, M.G., 2015, Origin of Eocene volcanic rocks at the south end of the Deer Lodge Valley, Montana, in Mosolf, J., and McDonald, C., eds., *40th annual field conference, Geology of the Elliston area, Montana and other papers: Northwest Geology*, v. 44, p. 201–212.
- Sears, J.W., McDonald, C., and Lonn, J., 2010, Lewis and Clark Line, Montana: Tectonic evolution of a crustal-scale flower structure in the Rocky Mountains, in Morgan, L.A., and Quane, S.L., eds., *Through the generations: Geological and anthropogenic field excursions in the Rocky Mountains from modern to ancient: Geological Society of America Field Guide* 18, p. 1–20.
- Sillitoe, R.H., Graubeger, G.L., and Elliott, J.E., 1985, A diatreme-hosted gold deposit at Montana Tunnels, Montana: *Economic Geology* v. 80, p. 1707–1721.
- Stacey, J.S., and Kramers, J.D., 1975, Approximation of terrestrial lead isotope evolution by a two-stage model: *Earth and Planetary Science Letters*, v. 26, p. 207–221.

- Tilling, R., Klepper, M., and Obradovich, J., 1968, K-Ar ages and time span of emplacement of the Boulder Batholith, Montana: *American Journal of Science*, v. 266, p. 671–689.
- Tosdal, R.M., Wooden, J.L., and Bouse, R.M., 1999, Pb isotopes, ore deposits, and metallogenic terranes, in Lambert, D.D., and Rutz, J., eds., *Application of radiogenic isotopes to ore deposits research and exploration: Reviews in Economic Geology*, v. 12, p. 1–28.
- Unruh, D.M., Fey, D.L., and Church, S.E., 2000, Chemical data and lead isotopic compositions of geochemical baseline samples from streambed sediments and smelter slag, lead isotopic compositions in fluvial tailings, and dendrochronology results from the Boulder River watershed, Jefferson County, Montana: U.S. Geological Survey Open-File Report 00-038, 75 p.
- Zartman, R.E., 1974, Lead isotopic provinces in the Cordillera of the western United States and their geologic significance: *Economic Geology*, v. 69, p. 792–805.
- Zartman, R.E., 1992, Archean crustal lead in the Helena embayment of the Belt Basin, Montana, in Bartholomew, M.J., Hyndman, D.W., Mogk, D.W., and Mason, R., eds., *International conference on basement tectonics, Proceedings of the eighth international conference on basement tectonics*, Butte, Montana, USA: August, 1988, p. 699–710.
- Zartman, R.E., and Doe, B.R., 1981, Plumbotectonics—The model: *Tectonophysics*, v. 75, p. 135–162.
- Zartman, R.E., and Haines, S.M., 1988, The plumbotectonics model for Pb isotopic systematics among major terrestrial reservoirs—A case for bi-directional transport: *Geochimica et Cosmochimica*, v. 52, p. 1327–1339.
- Zartman, R.E., and Stacey, J.S., 1971, Lead isotopes and mineralization ages in Belt Supergroup rocks, northwestern Montana and northern Idaho: *Economic Geology*, v. 66, p. 849–860.
- Zimmerman, J.L., 2016, Re-examination of ore-forming processes in the Emery mining district, Powell County, Montana: Butte, Montana Tech, M.S. thesis, 127 p.

## APPENDIX A

Summary of lead isotope data for intrusions, volcanic rocks and base metal vein galena assumed near zero U/Pb for galena samples from this investigation.

<b>Galena Sample No.</b>	<b>Host Rock</b>	<b>Mine/Location</b>	<b>District</b>	$^{206}\text{Pb}/^{204}\text{Pb}$	$^{207}\text{Pb}/^{204}\text{Pb}$	$^{208}\text{Pb}/^{204}\text{Pb}$
BF-48	Butte Granite	St. Anthony	Big Foot	17.92	15.57	38.10
E-42	Andesite	Emery	Emery	18.44	15.61	38.34
LC-37	Dacite	Ruby	lowland	18.34	15.59	38.43
LV-1	Andesite	Caved shaft	Leadville	17.80	15.55	37.93
BA-1	Butte granite	Morning	Basin	17.89	15.58	38.15
BO-2	Butte granite	Prospect Pit, Boomerang Gulch	Boulder	18.12	15.59	38.25
CL-1	Butte granite	Caved mine, head of Middle Fork Warm Springs Creek	Clancy	18.17	15.58	38.21
CO-1	Rhyolite	Montana Tunnels	Colorado	21.47	15.91	40.38
EH-2	Marble	Elkhorn	Elkhorn	18.21	15.62	38.36
ELS-14	Butte granite	Shaft, head of Bryan Creek	Elliston	18.32	15.59	38.29
RE-2	Butte granite	Shaft, head of Banner Creek	Rimini	17.89	15.55	38.01
WI-1	Andesite	East Pacific	Park	18.09	15.58	37.78
WI-2	Granodiorite	Kleinschmidt	Park	18.12	15.60	37.83
WI-5	Andesite	Marietta	Park	18.11	15.57	37.77
SC-2	Granodiorite	Hopeful	Scratchgravel Hills	17.54	15.52	37.16
MY-1	Sandstone	Empire	Marysville	17.89	15.53	37.73
TZ-1	Andesite	Big Tizer Wildcat	Wilson-Tizer	18.02	15.56	38.05
<b>Whole Rock</b>						
<b>No.</b>	<b>Rock Type</b>	<b>Formation</b>		$^{206}\text{Pb}/^{204}\text{Pb}$	$^{207}\text{Pb}/^{204}\text{Pb}$	$^{208}\text{Pb}/^{204}\text{Pb}$
KCS-15-63	Vitrophyre	Elkhorn Mt. Vol.		18.05	15.57	38.33
KCS-13-58	Vitrophyre	Lowland Crk. Vol.		17.50	15.51	37.83
KCS-14-20	Hornblende diorite	Elkhorn Mt. Intrusion		18.35	15.51	38.29
KCS-14-83	Diorite	Elkhorn Mt. Intrusion		17.88	15.57	38.46
GS-1	Diorite	Golden Sunlight	Whitehall	17.93	15.48	38.00

Factors used for correcting lead isotope data based on multiple analysis of NIST standard SEM-981. Accepted NIST standard SEM-981 values for  $^{206}\text{Pb}/^{204}\text{Pb} = 16.9405$ ,  $^{207}\text{Pb}/^{204}\text{Pb} = 15.4963$ , and  $^{208}\text{Pb}/^{204}\text{Pb} = 36.7219$ .

<b>Sample Number</b>	<b><math>^{206}\text{Pb}/^{204}\text{Pb}</math> Correction</b>	<b><math>^{206}\text{Pb}/^{204}\text{Pb}</math> Mean</b>	<b><math>^{207}\text{Pb}/^{204}\text{Pb}</math> Correction</b>	<b><math>^{207}\text{Pb}/^{204}\text{Pb}</math> Mean</b>	<b><math>^{208}\text{Pb}/^{204}\text{Pb}</math> Correction</b>	<b><math>^{208}\text{Pb}/^{204}\text{Pb}</math> Mean</b>
BF-48	1.0013	16.9178	1.0020	15.4657	1.0028	36.6180
E-42	1.0013	16.9178	1.0020	15.4657	1.0028	36.6180
LC-37	1.0013	16.9178	1.0020	15.4657	1.0028	36.6180
LV-1	1.0013	16.9178	1.0020	15.4657	1.0028	36.6180
BA-1	1.0012	16.9207	1.0017	15.4701	1.0025	36.6320
BO-2	1.0012	16.9207	1.0017	15.4701	1.0025	36.6320
CL-1	1.0012	16.9207	1.0017	15.4701	1.0025	36.6320
CO-1	1.0012	16.9207	1.0017	15.4701	1.0025	36.6320
EH-2	1.0012	16.9207	1.0017	15.4701	1.0025	36.6320
ELS-14	1.0012	16.9207	1.0017	15.4701	1.0025	36.6320
RE-2	1.0012	16.9207	1.0017	15.4701	1.0025	36.6320
WI-1	1.0011	16.9225	1.0016	15.4716	1.0023	36.6394
WI-2	1.0011	16.9225	1.0016	15.4716	1.0023	36.6394
WI-5	1.0011	16.9225	1.0016	15.4716	1.0023	36.6394
SC-2	1.0011	16.9225	1.0016	15.4716	1.0023	36.6394
MY-1	1.0011	16.9225	1.0016	15.4716	1.0023	36.6394
TZ-1	1.0011	16.9225	1.0016	15.4716	1.0023	36.6394
KCS-15-63	1.0012	16.9207	1.0017	15.4701	1.0025	36.6320
KCS-13-58	1.0012	16.9207	1.0017	15.4701	1.0025	36.6320
KCS-14-20	1.0013	16.9178	1.0020	15.4657	1.0028	36.6180
KCS-14-83	1.0013	16.9178	1.0020	15.4657	1.0028	36.6180
GS-1	1.0025	16.8986	1.0035	15.4418	1.0049	36.5436

## APPENDIX B

Lead isotope data corrected to initial lead for the Boulder batholith, satellite plutons, Lowland Creek and Elkhorn Mountains volcanic rocks from Doe and others (1968).

Sample Type	Formation	Location	$^{206}\text{Pb}/^{204}\text{Pb}$	$^{207}\text{Pb}/^{204}\text{Pb}$	$^{208}\text{Pb}/^{204}\text{Pb}$
K-feldspar	Unionville	Type locality	18.01	15.60	38.26
	Granodiorite				
K-feldspar	Unionville	Benchmark 4589	18.02	15.64	38.26
	Granodiorite	Clark Gulch Road			
K-feldspar	Unionville	Clark Gulch Road	18.02	15.63	38.28
	Granodiorite				
K-feldspar	Unionville	Aplite dike cutting granodiorite	17.89	15.64	38.40
	Granodiorite				
K-feldspar	Sheet alaskite	Schroeder Ranch	18.17	15.68	38.57
plagioclase	Sheet alaskite	Schroeder Ranch	18.10	15.58	38.34
K-feldspar	Sheet alaskite	Lowland Creek Road	18.14	15.58	38.33
K-feldspar	Pegmatite stringer	Kain quarry	17.97	15.60	38.25
K-feldspar	Pegmatite pod	Butte quartz monzonite	18.02	15.56	38.22
K-feldspar	Dike	Butte quartz monzonite	18.11	15.63	38.41
K-feldspar	Homestake	Quartz monzonite abandoned quarry	17.91	15.58	38.11
K-feldspar	Clancy	Kain quarry, type locality	17.99	15.60	38.23
	Granodiorite				
Whole rock	Clancy	Kain quarry, type locality	18.01	15.56	38.22
	Granodiorite				
K-feldspar	Butte quartz monzonite	Schroeder ranch	18.09	15.65	38.45
K-feldspar	Butte quartz monzonite	Homestake Pass, abandoned quarry	17.90	15.58	38.13
			17.91	15.58	38.13
			17.89	15.57	38.12
K-feldspar	Butte quartz monzonite	Equigranular facies	18.10	15.65	38.51
K-feldspar	Butte quartz monzonite	Equigranular facies	18.02	15.54	38.14
K-feldspar	Butte quartz monzonite	Strongly porphyritic	17.87	15.60	38.11
Glass	Lowland Creek volcanic field	Rhyolite, east of Spotted Dog Reservoir	18.66	15.70	38.67
K-feldspar	Lowland Creek volcanic field	Rhyolite, east of Spotted Dog Reservoir	18.57	15.68	38.54
Glass	Lowland Creek volcanic field	Crystal-rich vitrophyre, Sheeps Head Mountain	18.36	15.64	38.61
Glass	Lowland Creek volcanic field	Vitrophyre unit, base of Sheeps Head Mountain	18.20	15.67	38.45
Glass	Lowland Creek volcanic field	Vitrophyre from middle flow Sheeps Head Mountain	18.01	15.57	38.57
Plagioclase	Lowland Creek volcanic field	Middle flow Sheeps Head Mountain	18.15	15.64	38.64
Glass	Elkhorn Mountains volcanic field	Biotitic perlite west of Jefferson School	18.16	15.59	38.27
			18.16	15.62	38.41
Glass	Elkhorn Mountains volcanic field	Glassy welded tuff, Wolf Creek	18.18	15.65	38.53

## APPENDIX C

Lead isotope data from Zartman (1992) for sulfide veins hosted by the LaHood and Newland Formations, Belt Supergroup, and whole-rock lead isotope analysis from the LaHood, Newland, and Greyson Formations corrected for 1,400 million years of *in situ* radioactive decay.

Location	Formation	Analysis	$^{206}\text{Pb}/^{204}\text{Pb}$	$^{207}\text{Pb}/^{204}\text{Pb}$	$^{208}\text{Pb}/^{204}\text{Pb}$
Jefferson Canyon, Jefferson County	LaHood	Whole rock	16.78	15.81	36.22
Jefferson Canyon, Jefferson County	LaHood	Whole rock	16.32	15.60	35.33
Highland Mts., Silver Bow County	LaHood	Whole rock	17.18	15.59	45.13
Highland Mts., Silver Bow County	Newland	Whole rock	10.73	14.92	29.83
Highland Mts., Silver Bow County	Greyson	Whole rock	16.65	15.41	36.15
Bridger Range, Gallatin County	LaHood	Sulfide vein galena	17.13	15.81	37.11
Bridger Range, Gallatin County	LaHood	Sulfide vein galena	16.98	15.81	36.89
Highland Mts., Silver Bow County	Newland	Sulfide vein galena	16.82	15.67	36.47
Highland Mts., Silver Bow County	Newland	Sulfide vein galena	16.81	15.70	36.50
Little Belt Mts., Meagher County	Newland	Sulfide vein galena	16.74	15.59	36.50
Little Belt Mts., Meagher County	Newland	Sulfide vein galena	16.75	15.60	36.52
Little Belt Mts., Meagher County	Newland	Sulfide vein galena	16.70	15.57	36.47

Uncorrected present-day lead isotope data from Zartman (1992) for LaHood, Newland, and Greyson Formations.

Location	Formation	Analysis	$^{206}\text{Pb}/^{204}\text{Pb}$	$^{207}\text{Pb}/^{204}\text{Pb}$	$^{208}\text{Pb}/^{204}\text{Pb}$
Jefferson Canyon, Jefferson County	LaHood	Whole rock	17.88	15.88	37.06
Jefferson Canyon, Jefferson County	LaHood	Whole rock	18.99	15.87	37.93
Highland Mts., Silver Bow County	LaHood	Whole rock	22.70	16.08	61.54
Highland Mts., Silver Bow County	Newland	Whole rock	20.14	15.75	39.57
Highland Mts., Silver Bow County	Greyson	Whole rock	19.31	15.64	38.89

## APPENDIX D

Lead isotopes for Lowland Creek Volcanics from Dudás and others (2010).

<b>Rock Type</b>	<b><math>^{206}\text{Pb}/^{204}\text{Pb}</math></b>	<b><math>^{207}\text{Pb}/^{204}\text{Pb}</math></b>	<b><math>^{208}\text{Pb}/^{204}\text{Pb}</math></b>
Andesite	18.15	15.58	38.33
Dacite	16.86	15.39	37.74
Rhyodacite	18.15	15.57	38.27
Dacite vitrophyre	16.90	15.38	37.71
Tuff	18.30	15.58	38.37
Tuff, lower welded tuff	18.21	15.59	38.37
Tuff, lower basal ignimbrite	18.28	15.61	38.47
Tuff, welded	18.38	15.59	38.46
Tuff, welded	18.37	15.58	38.42
Tuff, crystal lithic	17.74	15.55	38.19
Tuff, partially welded	18.98	15.64	38.98
Dacite porphyry	17.04	15.43	38.02
Dacite porphyry	18.14	15.56	38.27
Dacite	18.17	15.57	38.31
Rhyolite	18.35	15.59	38.45
Tuff, upper welded	17.69	15.52	38.31
Dacite breccia	18.38	15.58	38.25
Andesite	17.67	15.54	38.34
Tuff welded	18.27	15.60	38.40
Rhyolite intrusion	18.32	15.60	38.32
Rhyolite intrusion	18.00	15.56	38.12

## APPENDIX E

Lead isotope data corrected to initial Pb isotope ratios using an age of 66 Ma for associated altered and mineralized rocks and intrusions for the Big Belt Mountains from du Bray and others (2017).

Formation	<sup>206</sup> Pb/ <sup>204</sup> Pb	<sup>207</sup> Pb/ <sup>204</sup> Pb	<sup>208</sup> Pb/ <sup>204</sup> Pb
Hornblende quartz monzonite of Mount Edith	17.95	15.47	37.80
Hornblende quartz monzonite of Mount Edith	17.79	15.45	37.65
Hornblende quartz monzonite of Mount Edith	17.88	15.47	37.71
Core/inner zone Boulder Baldy pluton: biotite granodiorite	16.82	15.34	37.11
Core/inner zone Boulder Baldy pluton: biotite granodiorite	16.77	15.31	37.03
Intermediate zone Boulder Baldy pluton: hornblende quartz monzodiorite	17.74	15.43	37.66
Intermediate zone Boulder Baldy pluton: hornblende quartz monzodiorite	17.94	15.44	37.74
Outer zone Boulder Baldy pluton: monzodiorite, magmatic texture	18.55	15.53	38.03
Outer zone Boulder Baldy pluton: aegirine quartz monzonite partially recrystallized	18.69	15.53	38.23
Aplite from outer zone of Boulder Baldy pluton	18.49	15.57	38.33
Feldspar Boulder Baldy pluton	18.45	15.51	38.13
Feldspar Boulder Baldy pluton	18.43	15.52	38.19
Weakly mineralized granodiorite/quartz monzodiorite of Miller Mountain	17.63	15.42	37.84
Feldspar porphyry south of Mount Edith	17.79	15.48	37.72
Proterozoic lamprophyre dike	18.75	15.61	38.58
A weakly mineralized rock from Porcupine prospect; iron oxide stained	17.87	15.54	37.55
Fluorite-Normandy prospect	18.25	15.53	38.03
Mineralized hornblende quartz monzodiorite east of Porcupine prospect	18.33	15.50	38.02
Vein in Mesoproterozoic Newland Formation, massive	18.16	15.58	37.68
Vein in Mesoproterozoic Newland Formation, iron oxide stained	20.80	15.73	39.65
Mineralized Mesoproterozoic Newland north of Boulder Baldy	17.66	15.54	37.16
Mineralized Mesoproterozoic Newland at Bigler prospect	18.29	15.58	37.73
Mineralized Mesoproterozoic Newland at Snowbank prospect	18.26	15.51	38.04
Mesoproterozoic Newland Formation	19.87	15.78	37.93

Uncorrected present day lead isotope data for altered, mineralized rocks, and intrusions for the Big Belt Mountains from duBray and others (2017).

<b>Formation</b>	<b><sup>206</sup>Pb/<sup>204</sup>Pb</b>	<b><sup>207</sup>Pb/<sup>204</sup>Pb</b>	<b><sup>208</sup>Pb/<sup>204</sup>Pb</b>
Hornblende quartz monzonite of Mount Edith	17.99	15.48	37.86
Hornblende quartz monzonite of Mount Edith	17.90	15.45	37.79
Hornblende quartz monzonite of Mount Edith	17.91	15.47	37.77
Core/inner zone Boulder Baldy pluton: biotite granodiorite	16.86	15.34	37.16
Core/inner zone Boulder Baldy pluton: biotite granodiorite	16.81	15.31	37.06
Intermediate zone Boulder Baldy pluton: hornblende quartz monzodiorite	17.80	15.43	37.74
Intermediate zone Boulder Baldy pluton: hornblende quartz monzodiorite	18.00	15.44	37.80
Outer zone Boulder Baldy pluton: quartz monzonite, magmatic texture	18.85	15.54	38.92
Outer zone Boulder Baldy pluton: monzodiorite, magmatic texture	18.65	15.53	38.26
Outer zone Boulder Baldy pluton: aegirine quartz monzonite, partially recrystallized	18.79	15.53	38.42
Outer zone Boulder Baldy pluton: quartz syenite, recrystallized and metasomatized	18.75	15.57	38.51
Aplite from outer zone of Boulder Baldy pluton	18.57	15.57	38.42
Feldspar Boulder Baldy pluton	18.51	15.51	38.18
Feldspar Boulder Baldy pluton	18.59	15.53	38.27
Weakly mineralized granodiorite/quartz monzodiorite of Miller Mountain	17.66	15.42	37.90
Feldspar porphyry south of Mount Edith	17.87	15.48	37.85
Proterozoic lamprophyre dike	18.83	15.61	38.71
A weakly mineralized rock from Porcupine prospect; iron oxide stained	17.88	15.54	37.56
Fluorite-Normandy prospect	18.27	15.53	38.05
Mineralized hornblende quartz monzodiorite east of Porcupine prospect	18.42	15.50	38.22
Vein in Mesoproterozoic Newland Formation, massive	18.26	15.58	37.75
Vein in Mesoproterozoic Newland Formation, iron oxide stained	22.40	15.80	41.09
Mineralized Mesoproterozoic Newland north of Boulder Baldy	17.72	15.55	37.22
Mineralized Mesoproterozoic Newland at Bigler prospect	18.41	15.59	37.92
Mineralized Mesoproterozoic Newland at Snowbank prospect	18.31	15.52	38.05
Mesoproterozoic Newland Formation	20.50	15.81	38.71

## APPENDIX F

Lead isotope data for streambed sediments, contaminated fluvial mill tails, and uncontaminated overbank fluvial mill tailings from the Basin mining district, Jefferson County, Montana. Data summarized from Unruh and others (2000).

<b>Sample Site</b>	<b>Sample Type</b>	<b><sup>206</sup>Pb/<sup>204</sup>Pb</b>	<b><sup>207</sup>Pb/<sup>204</sup>Pb</b>	<b><sup>208</sup>Pb/<sup>204</sup>Pb</b>
Boulder River	Stream terrace	18.19	15.58	38.25
Boulder River	Stream terrace	17.73	15.53	37.73
Boulder River	Stream terrace	18.07	15.57	38.15
Boulder River	Stream terrace	18.09	15.58	38.20
Boulder River	Stream terrace	18.10	15.59	38.23
Boulder River	Stream terrace	18.11	15.57	38.21
Basin Creek	Sediment core	18.05	15.57	38.10
Basin Creek	Sediment core	18.10	15.56	38.10
Basin Creek	Sediment core	18.13	15.57	38.12
Basin Creek	Sediment core	18.10	15.56	38.16
Basin Creek	Sediment core	18.12	15.56	38.12
Jack Creek	Sediment core	18.16	15.58	38.26
Jack Creek	Sediment core	18.09	15.58	38.24
Jack Creek	Sediment core	18.03	15.55	38.13
Jack Creek	Sediment core	18.10	15.58	38.21
Uncle Sam Gulch	Sediment core	17.99	15.58	38.16
High Ore Creek	Sediment core	18.08	15.56	38.17
High Ore Creek	Sediment core	18.10	15.57	38.23
High Ore Creek	Sediment core	18.02	15.56	38.16
Jack Creek	Fluvial mill tailings	17.92	15.56	37.99
Grub Gulch	Fluvial mill tailings	17.90	15.55	38.03
Uncle Sam Gulch	Fluvial mill tailings	17.92	15.56	38.02
High Ore Creek	Fluvial mill tailings	18.07	15.55	38.12
Jack Creek	Fluvial mill tailings	17.90	15.54	37.98
Jack Creek	Overbank fluvial mill tailings	17.93	15.56	38.00
Jack Creek	Overbank fluvial mill tailings	17.92	15.56	38.00
Jack Creek	Overbank fluvial mill tailings	17.99	15.58	38.13